Crumbs is an essential regulator of cytoskeletal dynamics and cell-cell adhesion during dorsal closure in *Drosophila*

David Flores-Benitez, Elisabeth Knust

DOI: http://dx.doi.org/10.7554/eLife.07398

Cite as: eLife 2015;10.7554/eLife.07398

Received: 10 March 2015
Accepted: 6 November 2015
Published: 6 November 2015

Crumbs is an essential regulator of cytoskeletal dynamics and cell-cell adhesion during dorsal closure in *Drosophila*

David Flores-Benitez and Elisabeth Knust*

Max-Planck-Institute of Molecular Cell Biology and Genetics,
Pfotenhauerstrasse 108
01307-Dresden, Germany

*Corresponding author
Tel: +49-351-210-1300
Fax: +49-351-210-1309
e-mail: knust@mpi-cbg.de

Keywords

Crumbs, amnioserosa, dorsal closure

Abstract (max 150 words)

The evolutionarily conserved Crumbs protein is required for epithelial polarity and morphogenesis. Here we identify a novel role of Crumbs as a negative regulator of actomyosin dynamics during dorsal closure in the *Drosophila* embryo. Embryos carrying a mutation in the FERM (protein **4**.1/**e**zrin/**r**adixin/**m**oesin) domain-binding motif of Crumbs die due to an overactive actomyosin network associated with disrupted adherens junctions. This phenotype is restricted to the amnioserosa and does not affect other embryonic epithelia. This function of Crumbs requires *D*Moesin, the Rho1-GTPase, class-I p21-activated kinases and the Arp2/3 complex. Data presented here point to a critical role of Crumbs in regulating actomyosin dynamics, cell junctions and morphogenesis.

Introduction

Dorsal closure (DC) in the *Drosophila* embryo is an established model for epithelial morphogenesis. The power of *Drosophila* genetics and cell biological tools have contributed to understand how signalling pathways, cell polarity and cell adhesion regulate the coordinated movements of two epithelial sheets, the epidermis and the amnioserosa (AS), a transient extraembryonic tissue [reviewed in (Ríos-Barrera and Riesgo-Escovar, 2013)]. More recently, elaborate biophysical techniques combined with high resolution imaging have elucidated how contractile forces are coordinated between cells in order to drive coherent changes in tissue morphology (Sokolow et al., 2012; Jayasinghe et al., 2013; Fischer et al., 2014; Wells et al., 2014; Eltsov et al., 2015; Saias et al., 2015). DC is a complex morphogenetic process taking about 2 hours, during which the epidermis expands dorsally to encompass the embryo. The process can be subdivided into three phases: i) elongation of the dorsal-most epidermal cells (DME) along the dorso-ventral axis; ii) contraction of AS cells and migration of the lateral epidermal cells towards the dorsal midline; iii) "zippering", i.e. adhesion of the epidermal cells from both sides on the dorsal midline [reviewed in (Gorfinkiel et al., 2011)]. Several forces contribute to these processes. First, pulsed contraction of AS cells produces a pulling force. These pulsed contractions are correlated with dynamic apical actomyosin foci, which transiently form in the apical medial cytocortex (Kiehart et al., 2000; Hutson et al., 2003; Solon et al., 2009; Gorfinkiel et al., 2009; Blanchard et al., 2010; Heisenberg and Bellaiche, 2013). Cells delaminating from the AS contribute additional pulling forces (Muliyil et al., 2011; Sokolow et al., 2012; Toyama et al., 2008). Second, a supracellular actomyosin cable, formed in the DME cells, surrounds the opening and provides contractile forces (Hutson et al., 2003; Rodriguez-Diaz et al., 2008). Finally, "zippering" of the two lateral epithelial sheets occurs, mediated by dynamic filopodia and lamellipodia (Eltsov et al., 2015; Jacinto et al., 2000).

A plethora of proteins contribute to coordinate this highly dynamic morphogenetic process. Beside transcription factors, these include adhesion molecules and signalling pathways, a variety of cytoskeletal proteins and their regulators. Non-muscle myosin-II heavy chain (MHC) and the non-muscle myosin regulatory light chain (MRLC), encoded by *zipper* (*zip*) and *spaghetti-squash* (*sqh*), respectively, are, together with the essential light chain, part of a force-producing molecular motor during DC [reviewed in (Vicente-Manzanares et al., 2009; Liu and Cheney, 2012)]. The small G-proteins of the Rho family, namely Rho1, Rac1, Rac2, Mtl, and Cdc42, regulate actomyosin activity and cell-cell adhesion (Abreu-Blanco et al., 2014; Magie et al., 1999; 2002). These GTPases stimulate myosin contraction through Rho-kinase (Rok) (Mizuno et al., 1999; Harden et al., 1999) or p21-activated kinase (*D*Pak) (Harden et al., 1996; Conder et al., 2004; Hofmann et al., 2004). They also modulate the Arp2/3 complex, which consists of seven subunits conserved in almost all eukaryotes (Rotty et al., 2013; Veltman and Insall, 2010).The Arp2/3 complex promotes the formation of densely branched, rapidly treadmilling actin filament arrays that, together with the Wiskott-Aldrich syndrome protein (WASP) and the

WASP-family verprolin-homologous protein (WAVE), coordinate membrane-cytoskeleton dynamics (Lecuit et al., 2011; Kurisu and Takenawa, 2009; Blanchoin et al., 2014). The Arp2/3 complex also regulates endocytosis of *D*E-cadherin (Georgiou et al., 2008; Leibfried et al., 2008) and thus contributes to the regulation of the *zonula adherens* (ZA), an adhesion belt encircling the apex of epithelial cells (Tepass et al., 1996; McEwen et al., 2000; Sarpal et al., 2012). Moreover, the *Drosophila* WAVE homolog SCAR, the main activator of Arp2/3 in fly embryos (Zallen et al., 2002), is a downstream effector of Rac, Cdc42 and *D*Pak (Lecuit et al., 2011; Kurisu and Takenawa, 2009). *D*Pak, in turn, can also activate the Arp2/3 complex independently of SCAR (Lecuit et al., 2011; Kurisu and Takenawa, 2009; Zallen et al., 2002). Thus, the regulation of cell-cell adhesion and cytoskeleton activity is closely linked to each other.

During epithelial morphogenesis, mechanisms controlling cell polarity have to be set in place to ensure tissue integrity. One of the key regulators of epithelial cell polarity in the *Drosophila* embryo is the Crumbs protein complex. Its core components are the type I transmembrane protein Crumbs (Crb) and the scaffolding proteins Stardust (Sdt), *D*Lin-7 and *D*PATJ, which are conserved from flies to mammals [reviewed in (Bulgakova and Knust, 2009; Tepass, 2012)]. *Drosophila* embryos mutant for *crb* or *sdt* are unable to maintain apico-basal polarity in most of their epithelia (Tepass and Knust, 1990; 1993; Bachmann et al., 2001; Hong et al., 2001). This leads to a complete breakdown of tissue integrity due to failure in positioning and maintaining the ZA, followed by apoptosis in many tissues, e.g. the epidermis and the AS (Grawe et al., 1996; Tepass and Knust, 1990; 1993; Tepass, 1996). Comparable defects in epithelial integrity are observed in mice lacking Crb2 or Crb3 (Whiteman et al., 2014; Xiao et al., 2011; Szymaniak et al., 2015). Conversely, over-expression of *Drosophila* Crb can lead to an expansion of the apical membrane domain, both in embryonic epithelial cells (Wodarz et al., 1995) and in photoreceptor cells (Muschalik and Knust, 2011; Pellikka et al., 2002; Richard et al., 2009). These results define Crb as an important apical determinant of epithelial cells. Besides a role in epithelial cell polarity, *Drosophila crb* controls tissue size in imaginal discs by acting upstream of the Hippo pathway [reviewed in (Boggiano and Fehon, 2012; Genevet and Tapon, 2011)], regulates morphogenesis of photoreceptor cells and prevents light-dependent retinal degeneration [reviewed in (Bazellières et al., 2009; Bulgakova and Knust, 2009)].

Crb contains in its extracellular domain an array of epidermal growth factor-like repeats, interspersed by four laminin A globular domain-like repeats. Its small cytoplasmic portion of only 37 amino acids contains two highly conserved motifs, a C-terminal PDZ (**P**ostsynaptic density/**D**iscs large/**Z**O-1) domain-binding motif (PBM), -ERLI, which can bind the PDZ-domain of Sdt and *D*Par-6 (Li et al., 2014; Roh et al., 2002; Bulgakova et al., 2008; Bachmann et al., 2001; Hong et al., 2001; Kempkens et al., 2006; Ivanova et al., 2015), and a FERM (protein **4**.1/**e**zrin/**r**adixin/**m**oesin) domain-binding motif (FBM) (Klebes and Knust, 2000), which can directly interact with the FERM-domain of Yurt (Yrt), Expanded (Ex) and Moesin (Moe) (Laprise et al., 2006; Ling et

al., 2010; Wei et al., 2015). Our previous structure-function analysis of Crb using a fosmid-based approach revealed that the PBM is essential for the maintenance of cell polarity in embryonic epithelia (Klose et al., 2013). In contrast, the FBM is non-essential for normal development of most embryonic epithelia. At later stages of development, however, embryos with a mutation in the FBM fail to undergo DC (Klose et al., 2013). This phenotype now provides access to unravel additional functions of this highly conserved polarity regulator. Using live imaging and genetic analysis we elucidate a novel function of Crb as a key negative regulator of actomyosin dynamics during DC. Our results also further our understanding on the mechanisms that couple the regulation of the cytoskeleton and cell-cell adhesion with the control of embryonic morphogenesis.

Results

The FBM of Crb is essential for dorsal closure.

We previously showed (Klose et al., 2013) that a fosmid covering the entire *crb* locus, named *foscrb*, completely rescues the lethality caused by the lack of endogenous *crb*. We also showed that a variant, in which the conserved tyrosine$_{10}$ in the FERM-domain binding motif (FBM) is replaced by an alanine (*foscrb$_{Y10A}$* variant) does not rescue embryonic lethality. Interestingly, the fosCrb$_{Y10A}$ variant properly localises at the apical domain in most embryonic epithelia, which undergo normal morphogenesis (i.e. germ band elongation, salivary gland invagination). But later in development, germ band (GB) retraction, dorsal closure (DC) and head involution fail to occur properly (Klose et al., 2013). This indicated that the FBM of Crb fulfils a tissue- and stage-specific morphogenetic function in the embryo. Moreover, these defects appear to be independent of a putative Tyr phosphorylation, because another variant, in which the Y10 is replaced by a phenylalanine (*foscrb$_{Y10F}$*), completely rescues the embryonic lethality of *crb* mutants (Klose et al., 2013). To get a better understanding of the mechanisms by which Crb regulates these morphogenetic processes, we performed detailed *in vivo* analyses of embryos expressing the different fosmid variants together with a *DE-cad::GFP* or a *DE-cad::mTomato* knock-in allele (Huang et al., 2009) in a *crb* null background (*crb^{GX24}* or *crb^{11A22}*) (for simplicity, these are called *foscrb*, *foscrb$_{Y10A}$* and *foscrb$_{Y10F}$* from now on).

Because staging of embryos depends on morphological criteria, and *foscrb$_{Y10A}$* mutant embryos show morphological defects, we imaged control and mutant embryos always in parallel, and stages were classified according to elapsed time after egg collection, i.e., after equal developmental times (see Materials and Methods for details about staging and imaging). By the time *foscrb* embryos finish GB retraction (Figure 1A, Video 1), *foscrb$_{Y10A}$* embryos (Figure 1B, Video 2) exhibit major defects in GB retraction, as revealed by a highly disorganised amnioserosa (AS) in which individual AS cells could hardly be followed. While *foscrb* embryos proceed through DC (Figure 1C,E, Video 1), those expressing the *foscrb$_{Y10A}$* variant progressively lose the AS (Figure 1D,F) and ultimately fail to complete DC (Video 2). Embryos expressing the *foscrb$_{Y10F}$* variant complete DC similar as *foscrb* embryos (Figure 1-figure supplement 1), indicating that the Y10A mutation specifically affects the progress of DC.

Various mechanisms have been documented to contribute to DC, including elongation of the dorsal most epidermal (DME) cells (Riesgo-Escovar et al., 1996). This elongation occurs normally in *foscrb* embryos, as revealed by phosphotyrosine (PY) staining associated with the ZA (Figure 1G). In contrast the DME cells of *foscrb$_{Y10A}$* embryos do not elongate co-ordinately (Figure 1H). We analysed the localisation of Crb and *D*Patj at this stage. Both proteins are expressed at higher levels in the epidermis compared to the AS (Figure 1I-J'). In *foscrb* embryos, Crb (Figure 1I) and *D*Patj (Figure 1I') are mostly absent from the leading edge (LE –Figure 1I-I' arrowheads) of the DME cells. In contrast, in *foscrb$_{Y10A}$* embryos both Crb$_{Y10A}$ (Figure 1J, asterisks) and *D*Patj

(Figure 1J', asterisks) are detected at the LE, particularly in those cells that remain short, while both are removed in cells that elongate properly (Figure 1J,J', arrowheads). Thus proper elongation of the DME cells fails in *foscrb*$_{Y10A}$ embryos.

The FBM of Crb regulates filopodia formation and organisation of the supracellular actomyosin cable in the DME cells.

Besides elongation of the DME cells, a complex actomyosin machinery is established at their LE. The DME cells extend filopodia and lamellipodia that are essential for correct "zippering" (Young et al., 1993; Edwards et al., 1997; Jacinto et al., 2000; Eltsov et al., 2015). These filopodia, revealed by staining with an antibody against Stranded at Second [Sas (Denholm et al., 2005)], extend dorsally in *foscrb* embryos (Figure 2A arrow). In contrast, filopodia in *foscrb*$_{Y10A}$ embryos are disorganised and often absent (Figure 2B, empty arrowhead and arrowhead, respectively). This is confirmed by live imaging of embryos expressing a Venus-tagged Sas protein (Video 3). Filopodia of *foscrb*$_{Y10A}$ embryos are erratic, and some even appear to move out of the plane (Video 3, arrow in *foscrb*$_{Y10A}$ embryo), probably because of the loss of contact with the AS.

A key regulator of the number and length of filopodia during DC is the actin-elongation promoting protein Enabled (Ena) (Gates et al., 2007; Nowotarski et al., 2014; Bilancia et al., 2014; Homem and Peifer, 2009). Ena concentrates at the LE of DME cells in *foscrb* embryos (Figure 2C, arrows). In contrast, Ena is strongly reduced at the LE of *foscrb*$_{Y10A}$ embryos (Figure 2D, arrowhead). Localisation of Ena at the LE depends on the ZA–associated protein Polychaetoid (Pyd) (Choi et al., 2011). However, Pyd localisation at the ZA shows no major difference in *foscrb* and *foscrb*$_{Y10A}$ embryos (Figure 2-figure supplement 1A-B'''). The localisation of the formins Dia and DAAM, both involved in the growth of actin-based protrusions (Matusek et al., 2006; Homem and Peifer, 2008; Liu et al., 2010), is also similar in *foscrb* and *foscrb*$_{Y10A}$ embryos (Figure 2-figure supplement 1C-F). This suggests that different regulators of Ena are affected in *foscrb*$_{Y10A}$ mutant embryos.

In addition to filopodia, forces produced by a supracellular actomyosin cable at the LE contribute to DC (Franke et al., 2005; Hutson et al., 2003; Kiehart et al., 2000; Jacinto et al., 2002; Young et al., 1993). This supracellular cable, which contains actin (Figure 2E) and the non-muscle myosin II Zipper (Zip, Figure 2E'), is correctly formed in *foscrb* embryos (Figure 2E,E' arrows). However, it is virtually absent in *foscrb*$_{Y10A}$ embryos (Figure 2F,F', arrowheads). Live imaging experiments using a *zipper::GFP* protein trap line (Buszczak et al., 2007; Morin et al., 2001) reveal that Zip::GFP appears homogenously along the LE in *foscrb* embryos. In contrast, it randomly concentrates in some segments along the LE of *foscrb*$_{Y10A}$ embryos (Figure 2-figure supplement 2). Together, these results show that the FBM of Crb is important for the generation and maintenance of actin-based protrusions and the correct organisation of the supracellular actomyosin cable at the LE.

The formation of the actomyosin cable at the LE depends on the removal of the adhesion protein Echinoid (Ed) from the LE and the AS cells (Laplante and Nilson, 2011; Lin et al., 2007). As expected, Ed in *foscrb* embryos is distributed as in wild type embryos (Figure 2G, arrowheads mark Ed absence at the LE). However, in *foscrb*$_{Y10A}$ embryos, Ed levels are strongly reduced in the DME cells (Figure 2H, magenta overlay), even though the DME cells are still in contact with the AS, as revealed by PY staining (Figure 2H'). It has been suggested that the asymmetric distribution of Ed is essential to exclude the polarity protein Bazooka (Baz) away from the LE (Laplante and Nilson, 2011; Pickering et al., 2013). We found that, in contrast to *foscrb* embryos (Figure 2I, arrowhead), *foscrb*$_{Y10A}$ embryos preserve Baz at the LE of those cells that fail to elongate (Figure 2J, arrow). In addition, there is a general reduction of Baz at the junctions of the DME cells of *foscrb*$_{Y10A}$ embryos (Figure 2-figure supplement 3). Together, these results suggest that the FBM of Crb is important for Ed stability and hence Baz redistribution and amount in DME cells.

The asymmetric distribution of different proteins in the DME cells reflects the planar cell polarity of these cells, a feature that also includes the removal of septate junction (SJ) components from the LE (Kaltschmidt et al., 2002). We found that removal of Coracle (Cora), Discs Large (Dlg) and Yurt (Yrt) from the LE appears normal in the different fosmid variants (Figure 2-figure supplement 4), suggesting that not all aspects of the planar polarisation of the DME cells are affected in embryos expressing the *foscrb*$_{Y10A}$ variant.

Ed, Baz and *D*E-cadherin (*D*E-cad) are all proteins associated with the ZA, which is essential in maintaining adhesion between the dorsal epidermis and the AS and for transmitting the forces generated during DC (Gorfinkiel and Arias, 2007; Heisenberg and Bellaiche, 2013; Lecuit et al., 2011). In *foscrb*, *D*E-cad localises at all cell-cell contacts, including the LE (Figure 2K, arrow). In *foscrb*$_{Y10A}$ embryos, however, the *D*E-cad signal is strongly reduced at the LE (Figure 2L, solid arrowhead). Moreover, disruption of *D*E-cad suggests a discontinuous adhesion belt in the AS cells of these embryos (Figure 2L, empty arrowheads). The loss of *D*E-cad from the LE in the *foscrb*$_{Y10A}$ embryos at this early stage is different from the normal redistribution of *D*E-cad that occurs at late stages during the zippering phase (Gorfinkiel and Arias, 2007). As expected, in *foscrb*$_{Y10F}$ embryos, all proteins mentioned above localise as in *foscrb* embryos (Figure 2-figure supplement 5).

Taken together, these results show that the DC phenotype in *foscrb*$_{Y10A}$ embryos is accompanied by defects in the establishment of the complex actomyosin apparatus at the LE of the DME cells and by the disturbance or even loss of different components of the ZA (schematised in Figure 2M,N).

The FBM of Crb is essential for adhesion of the AS.

As described above, GB retraction is defective and the AS is strongly disorganised in *foscrb*$_{Y10A}$ embryos (Figure 1F). Because the AS is required during GB retraction (Lamka and Lipshitz, 1999; Lynch et al., 2013; Scuderi and Letsou, 2005), we analysed by live imaging whether the AS is affected before GB retraction.

In *foscrb* and *foscrb*$_{Y10A}$ embryos, at the beginning of stage 11, AS cells are elongated along the antero-posterior axis (Figure 3A,D), highlighted by *D*E-cad::mTomato along the ZA (Figure 3B,E, arrows). In *foscrb*$_{Y10A}$ embryos, however, the continuity of *D*E-cad::mTomato is frequently disrupted (Figure 3E, arrowhead) and *D*E-cad::mTomato additionally appears in large intracellular clusters of unknown identity (Figure 3E, concave arrowheads), which are never observed in *foscrb* embryos. As GB retraction proceeds, fragmentation of the ZA continues in the AS of *foscrb*$_{Y10A}$ embryos and the tissue disintegrates (Figure 3F arrowheads and Video 4; and for a dorsal view of a different set of embryos see Video 5), while the dorsal aspect of *foscrb* embryos is covered by a continuous epithelial sheet (Figure 3C).

The defects of the AS in *foscrb*$_{Y10A}$ embryos become very obvious in scanning electron micrographs (Figure 3-figure supplement 1). At stage 14, the AS forms a flat monolayer of epithelial cells in *foscrb* embryos (Figure 3-figure supplement 1A,A'). In contrast, in *foscrb*$_{Y10A}$ embryos developed for the same period of time, the AS is completely disorganised. Large processes form, some of which extend over the caudal end of the embryos (Figure 3-figure supplement 1B,B', arrow). Some isolated cells are visible over the epidermis (whether these are detached AS cells or migrating haemocytes was not determined –Figure 3-figure supplement 1B, arrowhead), while others have the appearance of apoptotic cells (Figure 3-figure supplement 1B', concave arrowhead).

Together, these observations suggest that cell-cell adhesion in the AS is strongly disrupted in *foscrb*$_{Y10A}$ embryos, and define the FBM of Crb as an important regulator of cytoskeletal organisation and cell-cell adhesion of the AS.

The FBM of Crb is essential for the integrity of the AS.

Our scanning electron microscopy analyses suggest that the AS of *foscrb*$_{Y10A}$ embryos undergo apoptosis. In order to determine whether apoptosis contributes to the disruption of the AS, we used the apoptotic reporter Apoliner, an RFP-GFP fusion protein localising at cell membranes of live cells. Caspase activation releases the GFP moiety, which is relatively unstable after cleavage, so dying cells have a stronger red appearance (Bardet et al., 2008; Kolahgar et al., 2011). Apoliner expression in the AS (specifically driven by the line GAL4$^{332.3}$) of *foscrb* embryos (Video 6) revealed some apoptotic cells at the posterior canthus at the end of GB retraction (Figure 4A, arrow). In *foscrb*$_{Y10A}$ embryos developed for the same period of time, more apoptotic cells are visible, some of which detach (Figure 4B, arrowheads), while others remain attached to the posterior edge of the remaining AS (Figure 4B, arrow). As DC progresses in *foscrb* embryos, some apoptotic cells delaminate from the AS and are easily distinguished (Video 6, blinking arrows –some of these cells could be hemocytes with engulfed apoptotic debris, as reported previously (Bardet et al., 2008)). At this stage, almost all AS cells in *foscrb*$_{Y10A}$ embryos are apoptotic (Video 6, compare embryos at 210 min). Finally, at the end of DC, the

internalised AS cells are localised in a central rod-like structure in *foscrb* embryos and subsequently die by apoptosis (Figure 4C) [as has been reported for wild type embryos (Reed et al., 2004; Shen et al., 2013)], while in $foscrb_{Y10A}$ embryos at this time point the remaining AS cells are completely disaggregated (Figure 4D). To summarise, the AS in $foscrb_{Y10A}$ embryos breaks apart and undergoes premature apoptosis (Video 6), supporting the conclusion that an intact FBM is required for maintaining the integrity of the AS.

Several other processes are required for proper DC and integrity of the AS. At early stages, specification of the AS requires the U-shaped-group of genes (*hindsight –hnt*, *tail-up –tup*, *u-shaped –ush*, and *serpent –srp*), mutations in which produce phenotypes similar to those observed in $foscrb_{Y10A}$ embryos (Frank and Rushlow, 1996; Lamka and Lipshitz, 1999; Yip et al., 1997; Scuderi and Letsou, 2005; Lynch et al., 2013). Hnt shows a strong and comparable expression pattern in the AS of *foscrb* and $foscrb_{Y10A}$ embryos at early and late stages (Figure 4-figure supplement 1), even in the detached AS cells of $foscrb_{Y10A}$ embryos (Figure 4-figure supplement 1D, arrowhead). This indicates that fate specification is not affected in $foscrb_{Y10A}$ embryos.

AS integrity also requires integrin-mediated attachment to the yolk sac membrane (Reed et al., 2004). Therefore, we analysed the localisation of integrin-β_{PS}, and found no major differences between *foscrb* and $foscrb_{Y10A}$ embryos (Figure 4-figure supplement 2A,B).

Yrt function is also important during DC, and zygotic *yrt* mutants have DC defects (Hoover and Bryant, 2002), similar to the ones observed upon Crb over-expression in the AS (Harden et al., 2002; Wodarz et al., 1995). Because Yrt is a FERM protein that negatively regulates Crb by directly interacting with its FBM (Laprise et al., 2006), Yrt appeared as a likely candidate in mediating the $foscrb_{Y10A}$ mutant phenotype. Yrt localises at the lateral domain and concentrates towards the apical aspect in a Crb-dependent manner from stage 13 onwards (Laprise et al., 2006). We found that independently of the fosmid genotype, Yrt concentrates correctly towards the apical aspect of the cells (Figure 4-figure supplement 3). Moreover, embryos expressing *foscrb* and lacking zygotic *yrt* show defects in DC mainly after GB retraction, when a failure in the zippering at the posterior canthus is patent (Video 7, arrow in the upper embryo). Despite this, the overall AS integrity is preserved during DC and most of the zippering is completed, leaving a hole only at the posterior canthus. This phenotype is completely different from the phenotype of $foscrb_{Y10A}$ embryos described above (Video 2). Significantly, embryos with both the zygotic *yrt* mutant allele and the $foscrb_{Y10A}$ variant do not show amelioration of the $foscrb_{Y10A}$ phenotype (Video 7, bottom embryo). These embryos show strong defects in GB retraction, and the integrity of the AS is lost as development progresses. These results show that the DC phenotype of $foscrb_{Y10A}$ embryos starts earlier in development and is more complex than that in *yrt* mutants, as the former fail in germ band retraction, lose the AS and do not progress on the zippering process. Thus, Yrt seems not to be involved in the phenotype of $foscrb_{Y10A}$ embryos.

The AS regulates aspects of DME differentiation (Stronach and Perrimon, 2001) and embryos carrying mutations in components of the JNK signalling pathway show defective elongation of DME cells and fail to establish the supracellular actomyosin cable at the LE (Riesgo-Escovar et al., 1996; Martín-Blanco et al., 1998; Ricos et al., 1999; Glise et al., 1995; Hou et al., 1997; Kockel et al., 1997; Reed et al., 2001; Ríos-Barrera and Riesgo-Escovar, 2013). The mutant phenotype described here is characterised by defects in both the AS and the DME cells. To assess whether defects in the DME observed in *foscrb*$_{Y10A}$ embryos are the result of impaired JNK signalling, we used the reporter line *puc-lacZ* (Martín-Blanco et al., 1998; Ring and Martinez Arias, 1993). At the beginning of DC, the DME cells of *foscrb* and *foscrb*$_{Y10A}$ embryos are β-gal positive (Figure 4E,F), with few *lacZ*-positive nuclei in the row of cells ventral to DME cells (Figure 4E,F, arrowheads). At advanced DC, *foscrb* embryos still show a single row of β-gal positive cells (Figure 4G), while in *foscrb*$_{Y10A}$ embryos β-gal positive nuclei can also be found at positions more ventral to the DME cells (Figure 4H, arrowheads). However, given that there is no significant difference in the number of β-gal positive nuclei along 50 μm of the dorsal epidermis between these genotypes (Figure 4G,H, brackets and 4K), we suggest that this phenotype is the result of aberrant elongation of the DME cells in *foscrb*$_{Y10A}$ embryos (see for example Figure 1H). Accordingly, at the time when *foscrb* embryos complete DC, these embryos (Figure 4I) and *foscrb*$_{Y10A}$ embryos exhibit a single row of β-gal positive cells on each side of the dorsal epidermis (Figure 4J). This is independent of whether the epidermis fuses on the dorsal midline (Figure 4J, encircled by dashed line), closes on the same side of the epidermis, thus causing bunching of the tissue (Figure 4J, encircled by dotted line) or does not touch any contra-lateral epidermis (Figure 4J, arrow). A normal activation of JNK signalling is also observed in *foscrb*$_{Y10F}$ embryos (Figure 4-figure supplement 4), showing that JNK signalling appears to be normal in the DME cells of *foscrb*$_{Y10A}$ embryos.

Taken together, these results support the conclusion that the FBM of Crb is an important regulator of the integrity and morphogenesis of the AS without affecting its specification during development.

The FBM of Crb controls actomyosin dynamics in the AS.

It has been previously shown that perturbing actomyosin dynamics of the AS cells interferes with normal DC (Solon et al., 2009; Gorfinkiel et al., 2009; Fischer et al., 2014). These dynamics, which are evident in stage 13 *foscrb* embryos (Video 8) similar as in wild-type embryos, is characterised by pulsed contractions of the AS cells. In *foscrb*$_{Y10A}$ embryos, however, the pulsed contraction are difficult to follow, since individual cells can hardly be distinguished due to the highly disrupted ZA (Video 8, compare Figure 5A and 5B). Pulsed-contraction of wild-type AS cells has been correlated with a regular appearance and disappearance of medial actomyosin foci (Blanchard et al., 2010; David et al., 2010; Solon et al., 2009). These actomyosin foci are

observed in *foscrb* embryos as revealed by Zip::GFP (Video 9 and Figure 5C). Kymographs show that these foci are transient and disassemble after contraction (Figure 5C',D'). In contrast, the AS of $foscrb_{Y10A}$ embryos shows more Zip::GFP foci (Figure 5D), some of which are more prominent (Figure 5D', and Figure 5-figure supplement 1 and Video 10). A similar behaviour was observed for F-actin (labelled with Utrophin::GFP (Rauzi et al., 2010) -data not shown). Importantly, analysis of the periodicity of foci formation shows that *foscrb* and $foscrb_{Y10F}$ embryos have similar pulsed contractions, while $foscrb_{Y10A}$ embryos have aberrant contractions, in that foci are more persistent (Figure 5E). These observations support the hypothesis that the AS of embryos expressing the Crb_{Y10A} variant is under both constant and uncoordinated contraction.

The activity of non-muscle myosin-II (Zip) is mainly regulated by the phosphorylation state of the myosin-regulatory light chain [reviewed in (Tan et al., 1992)], encoded by the gene *spaghetti squash* (*sqh*). Thus, if over-active actomyosin is responsible for the DC defects of $foscrb_{Y10A}$ embryos, we expect that expressing Flapwing (*flw*), the major *Drosophila* Sqh phosphatase (Vereshchagina et al., 2004), may suppress the DC defects. In fact, UAS-driven expression of Flw in the AS of $foscrb_{Y10A}$ embryos leads to a suppression of the DC phenotype (Figure 6D-F, Video 11), while it does not produce any evident dominant phenotype in *foscrb* or $foscrb_{Y10F}$ embryos (Figure 6A-C, and Figure 6-figure supplement 1). Interestingly, Flw over-expression also suppresses the disruption of the ZA in the AS (Video 12, compare B vs. D). This result supports our hypothesis that the FBM of Crb negatively regulates actomyosin activity in the AS.

Rho GTPases have been shown to stimulate myosin contraction by activating Rho-kinase (Rok) or the p21-activated kinase (*D*Pak), and are required for proper DC (Mizuno et al., 1999; Harden et al., 1999; 1996; Conder et al., 2004; Magie et al., 1999; 2002). To test whether Rho-GTPases are involved in the Crb-mediated DC phenotype, we expressed different versions of established Rho family effectors (see working model in Figure 6G) and examined their effects on DC in the embryonic cuticle, a suitable read-out of DC. We grouped the embryos according to their cuticle phenotype into two major categories (Figure 7A): 1) embryos with "DC-defect", which exhibit a range of defects from extensive dorsal opening (in which the mouthparts are exposed), to embryos with complete DC, which, however, still failed to hatch; and 2) embryos with "WT-like" cuticle, which includes all those that hatch (for more details about the different categories and phenotypes see Figure 7-figure supplement 1). Depending on the *crb* allelic combination, 89-98% of embryos expressing the $foscrb_{Y10A}$ variant fall into the "DC-defect" category (Figure 7A, 1^{st}-6^{th} black bars).

Using this read-out, we confirm that over-expression of the myosin phosphatase Flw in the AS strongly suppresses the DC defects of $foscrb_{Y10A}$ embryos. In fact, >75% hatch (Figure 7A, 10^{th} vs. 6^{th} bars) and even some $foscrb_{Y10A}$ adults eclose with no obvious defect (Figure 7C). Interestingly, cuticles from $foscrb_{Y10A}$ and hemi- or homozygous for the flw^{6} allele show an enhanced DC phenotype in comparison with the $foscrb_{Y10A}$ with a wild type *flw* allele (Figure 7A, 3^{rd} vs. 11^{th} black bars: 91.2% to 97.1%; and Figure 7-figure supplement 1, 3^{rd}

vs. 9th black bars, completely open cuticle from 27.7% to 73.5%). These results support the conclusion that the FBM of Crb regulates the AS actomyosin dynamics by regulating myosin activity.

In line with this conclusion we found that over-expression of dominant-negative Rho (Rho^{N19}) or a kinase-dead Rok (Rok-CAT-KG) in the AS of $foscrb_{Y10A}$ increases the number of hatched larvae (Figure 7A, 5th vs. 12th and 13th gray bars: from 2.9% to 13.4% and 10.0%, respectively), and the proportion of embryos with open cuticles is reduced (Figure 7-figure supplement 1, 5th vs 12th and 13th black bars, from 52.7% to 23.4% and 30.6%, respectively). Moreover, $Rho1^{1B}$ hemizygosity effectively suppresses the DC defects of $foscrb_{Y10A}$ embryos (Figure 7A, 14th bar vs. 1st black bars, 79.2 vs. 98.3%). In contrast, $foscrb_{Y10A}$ embryos hemi- or homozygous for rok^{2} show no suppression of the DC phenotypes (Figure 7A, 15th vs. 3rd bars), which suggests that *rok* deficiency may be deleterious in the $foscrb_{Y10A}$ background and that other morphological processes dependent on Rok could be affected (Simões et al., 2010; Krajcovic and Minden, 2012; Mason et al., 2013; Bertet et al., 2004). Similarly, over-expression of dominant-negative Rac1 ($Rac1^{N17}$) in the AS of $foscrb_{Y10A}$ embryos does not suppress the DC phenotype (Figure 7A, 16th vs. 5th bars) and even appears to increase the proportion of embryos with open cuticles (Figure 7-figure supplement 1, 5th vs. 16th black bars, from 52.7% to 72.9%). We assume that the phenotypic enhancement is due to an additive effect, since over-expression of $Rac1^{N17}$ in wild-type embryos results in DC defects (Harden et al., 2002).

An important regulator of cytoskeleton activity downstream of Rho GTPases is *D*Pak (Hofmann et al., 2004). Interestingly, over-expression of the auto-inhibitory domain of *D*Pak [*D*Pak-AID -(Conder et al., 2004)] in the AS of $foscrb_{Y10A}$ embryos leads to a very strong suppression of the DC phenotype, as 59% of those embryos hatch (Figure 7A, 17th vs. 6th bars), and even adult flies eclose (Figure 7D). Accordingly, over-expression of constitutive active *D*Pak (*D*Pak-myr) in the AS of otherwise viable *foscrb* embryos leads to embryonic lethality with >90% of embryos with a DC-defect (Figure 7A, 18th vs. 19th bars). These results indicate that unregulated activation of *D*Pak in the AS is sufficient to produce defects in DC, and that this kinase plays a major role in the defects observed in the $foscrb_{Y10A}$ embryos.

*D*Moe has been shown to antagonise the activity of the Rho pathway (Speck et al., 2003; Neisch et al., 2010; Hipfner et al., 2004). The participation of *D*Moe in the process under discussion here is supported by the fact that the FBM of Crb can recruit *D*Moesin (*D*Moe) to the membrane (Médina et al., 2002) and physically interacts with it (Wei et al., 2015), and that phosphorylated-*D*Moe (P-*D*Moe) is reduced in stage 11 $foscrb_{Y10A}$ embryos (Klose et al., 2013). This reduction in P-*D*Moe persists during DC (Figure 7-figure supplement 2). In line with this, over-expression of the phosphomimetic form $DMoe^{T559D}$ in the AS of $foscrb_{Y10A}$ embryos notably increases the number of larvae that hatch (Figure 7A, 6th vs. 20th gray bars, from 10.8% to 30.9%), while over-expression of *D*Moe does not ameliorate the DC defects in those embryos (Figure 7A, 21st bar). This suggests that the regulation of the cytoskeleton dynamics by Crb is mediated in part by the active form of *D*Moe.

Together these results let us to conclude, that the FBM of Crb regulates actomyosin dynamics in the AS during DC by down-regulating the activity of the Rho1 pathway.

We wanted to exclude the possibility that the phenotypes observed are due to a dominant effect of the Y10A mutation. In fact, over-expression of full-length Crb^{WT} in the AS of wild-type embryos leads to premature contraction of the AS and a DC phenotype (Harden et al., 2002; Wodarz et al., 1995). Driving the expression of UAS-Crb^{WT} in the AS of *foscrb$_{Y10A}$* embryos leads to a suppression of the DC phenotype, as >36% hatch at 18ºC (Figure 7A, 8th and 9th bars vs. 5th gray bars), while inducing a stronger over-expression by maintaining embryos at 29°C does not ameliorate the *foscrb$_{Y10A}$* phenotype (Figure 7A, 5th vs. 7th bars). These results show that the DC phenotype of *foscrb$_{Y10A}$* embryos is due to loss of Crb function.

The FBM of Crb is essential for the stability of *D*E-cadherin in the AS.

Besides an over-active actomyosin network, *foscrb$_{Y10A}$* embryos exhibit interruptions in *D*E-cad distribution (Figures 2L, 3F and 5B). In addition some embryos show weak head-involution defects (Figure 7-figure supplement 3), a phenotype reminiscent to that of weak alleles of *shotgun* (*shg*) (the gene encoding *D*E-cad) (Tepass et al., 1996), *armadillo* (*arm*) (the gene encoding β-catenin) (McEwen et al., 2000) or *α-Cat* (Sarpal et al., 2012). Therefore we asked whether the DC phenotype of *foscrb$_{Y10A}$* embryos could be rescued by restoring a functional adhesion belt. Over-expression of *D*E-cad in the AS of these embryos indeed can suppress the DC phenotype, as 70% of the larvae hatched (Figure 7A, 22nd vs. 6th bars), and even adult animals are obtained (Figure 7E).

A likely candidate of *D*E-cad regulation is the Arp2/3 complex, which has been shown to regulate endocytosis of *D*E-cad (Georgiou et al., 2008; Leibfried et al., 2008). In addition, reducing the activity of the Arp2/3 complex suppresses the DC phenotype of *α-Cat* mutants (Sarpal et al., 2012). Therefore, we tested the effects of removing one copy of *SCAR*, *Arp3* or *Arpc1* on the DC phenotype of *foscrb$_{Y10A}$* embryos. Strikingly, *foscrb$_{Y10A}$* embryos that are heterozygous for *SCAR$^{\Delta 37}$* exhibit only minor defects in GB retraction (Figure 8B), partially restore *D*E-cad::GFP localisation in the AS (compare Figure 8H with Figure 5B) and completed DC (Figure 8F, Video 13). In fact, ~28% of these larvae hatch, as revealed by the cuticle phenotype (Figure 7A, 23rd vs. 2nd bar), and even some of the *w;foscrb$_{Y10A}$,DE-cad::GFP/SCAR$^{\Delta 37}$,DE-cad::GFP;crb^{GX24}* develop into adult flies that exhibit defects in abdominal development (Figure 7F, arrowhead). A similar suppression was obtained in *foscrb$_{Y10A}$* embryos heterozygous for *Arp3^{EP3640}* (Video 14) (Figure 7A, 24th vs. 3rd bar). *foscrb* embryos heterozygous for *SCAR$^{\Delta 37}$ or Arp3^{EP3640}* show normal DC (Figure 8E and Video 14).

In summary we could demonstrate that the DC phenotype of embryos expressing Crb_{Y10A} is due to enhanced Rho-mediated actomyosin activity and reduced adhesion. Whether these two processes are linked or independent functions downstream of Crb remains to be discussed.

Discussion

Dorsal closure is an ideal model to study how coordinated behaviour of epithelial sheets controls morphogenesis. Here we present data to show that a mutation in the FERM-domain binding motif of the polarity determinant Crb affects major steps during DC, namely elongation of the DME cells, proper formation of the actomyosin cable at the LE, and regulated constriction of the AS cells. In addition, impaired *D*E-cad localisation suggest impaired adhesion. Overall, our results define a novel role of the FBM of Crb as an essential negative regulator of actomyosin dynamics in the AS during DC in *Drosophila*. This function is not allele-specific, since embryos carrying a *crb* allele, in which Y10, P12 and E16 in the FBM are replaced by alanines (Huang et al., 2009) develop a similar DC phenotype as $foscrb_{Y10A}$ embryos (data not shown). Genetic interaction studies revealed that this function of the FBM is mediated by *D*Moesin, members of the Rho family, the p21 activated kinase *D*Pak, and the SCAR-Arp2/3 complex (Figure 6G).

One phenotype observed upon complete loss of function of *crb* is a failure to maintain an intact ZA, a phenotype associated with the loss of polarity of many embryonic epithelia (Tepass et al., 1990; Tepass and Knust, 1990; 1993; Grawe et al., 1996; Tepass, 1996). In fact, the AS is the tissue that is affected earliest (late stage 7/early stage 8) in *crb* mutant embryos (Tepass, 1996). However, $foscrb_{Y10A}$ embryos exhibit disrupted *D*E-cad staining in the AS only from stage 11 onward. Therefore, we suggest that the way how Crb controls maintenance of ZA integrity in the AS at later stages is different from its early function, which depends on a functional PBM (Wodarz et al., 1993; Klose et al., 2013) and its interactions with the Par complex (Morais-de-Sá et al., 2010; Harris and Peifer, 2005). However, whether Crb, and in particular its FBM, regulates ZA integrity during DC by a different mechanism, or whether defects in the ZA are a secondary consequence of impaired actomyosin activity, remains to be determined.

Several of our results are compatible with the assumption that Crb regulates actomyosin dynamics, but since $foscrb_{Y10A}$ mutant embryos show defects both in the AS and the DME cells, we cannot distinguish in which of the tissues Crb activity is primarily required and whether defects observed in the DME of $foscrb_{Y10A}$ mutant embryos are secondary consequences of excessive contraction of the AS cells. Previous results clearly show that the activity of one tissue affects the behaviour of the respective other (Kiehart et al., 2000; Hutson et al., 2003; Gorfinkiel et al., 2009; Solon et al., 2009). For example, *zip* mutants have DC and head involution defects, and restoring *zip* function in either the dorsal epidermis or the AS is sufficient to rescue dorsal-open phenotypes (Franke et al., 2005). Similarly, expression of Pak-AID in the AS of $foscrb_{Y10A}$ mutants is sufficient to recover

proper elongation of the DME (data not shown). However, the multitude of phenotypes observed in the DME cells of *foscrb*$_{Y10A}$ mutant embryos, such as persistence of Crb$_{Y10A}$, *D*Patj and Baz proteins and decrease of Ed expression at the LE, as well as disruption of the supracellular actomyosin cable and disorganised filopodia, suggest that Crb performs also specific functions in the DME. One possibility is that Crb influences actomyosin activity and filopodia formation in the DME cells by regulating the stability and localisation of Ena, the major regulator of protrusive activity at the LE (Nowotarski et al., 2014). Another possibility is that Crb regulates the LE actomyosin by modulating the localisation of Baz. In wild-type embryos, the removal of Baz from the LE (Laplante and Nilson, 2011) allows the relocation of the lipid phosphatase Pten, which, in turn, results in a localised accumulation of phosphatidylinositol-3,4,5-trisphosphate at the LE, promoting the formation of filopodia along the LE (Pickering et al., 2013).

Crb regulates actomyosin dynamics

The most prominent phenotype of *foscrb*$_{Y10A}$ embryos is the over-contraction of AS cells, most likely mediated by *D*Pak. In fact, cortical localisation of *D*Pak in the AS of *foscrb*$_{Y10A}$ embryos appears to be increased in some cells (data not shown). In addition, over-expression of Pak-AID in the AS of *foscrb*$_{Y10A}$ suppresses the GB retraction and DC phenotypes. A similar degree of suppression was observed upon over-expression of Flw, a negative regulator of Sqh. Members of the Rho GTPase family are well-established upstream regulators of actomyosin dynamics. Our data suggest that Rho1 plays a crucial role downstream of Crb, since heterozygosity of *Rho1*^{1B} partially suppresses the DC phenotype of *foscrb*$_{Y10A}$ embryos. Previous data showed that over-expression of the constitutively active or dominant-negative form of Rac1 in the AS of wild-type embryos results in AS disruption (Harden et al., 2002). Our observation that the phenotype of *foscrb*$_{Y10A}$ embryos is enhanced upon expression of a dominant negative form of Rac1 in the AS of *foscrb*$_{Y10A}$ embryos suggests that Rac1 may act upstream of Crb or in a parallel pathway. Since the effects of dominant negative Cdc42^{N17} could not be studied due to technical difficulties (see Material and Methods), we cannot exclude any contribution of Cdc42 in this process. Therefore, our data so far support a role of Rho1 in the Crb-mediated control of actomyosin dynamics in the AS (Figure 6G).

The FERM protein *D*Moe is a likely candidate to link the FBM of Crb to Rho1 activity. *Dmoe* mutant imaginal epithelial cells lose epithelial markers and intercellular adhesion, become motile and show invasive behaviour (Speck et al., 2003). In addition, lack of *D*Moe activates the Rho1-Rok-myosin cascade and JNK-mediated apoptosis in imaginal discs (Warner et al., 2010; Neisch et al., 2010). In fact, the FBM of Crb can recruit Moe to the cell membrane, a process that fails upon replacement of Tyr10 or Arg7 by Ala in the FBM of Crb (Neisch et al., 2010; Médina et al., 2002). Similarly, mutating Tyr10 in the FBM of the intercellular adhesion molecule (ICAM)-2 or the equivalent Tyr residue in the FBM of the neural cell adhesion molecule L1

impairs interaction with the FERM proteins radixin and ezrin, respectively (Hamada et al., 2003; Cheng et al., 2005). Moreover, it has been shown recently that the FBM of Crb is necessary for organising *D*Moe, aPKC and the actin cytoskeleton at the marginal zone in the developing follicular epithelium (Sherrard and Fehon, 2015). And in cervical carcinoma cells, over-expression of the mammalian CRB3 protein restores an epithelial-like morphology by organising a cortical actomyosin network through the regulation of the p114RhoGEF-RhoA-ROCK1/2 pathway via the FERM protein Ehm2 (Loie et al., 2015). Finally, recent works documented direct binding between Moesin and Crb, which was abolished upon Y10A substitution (Wei et al., 2015).

It is unlikely that one of the other two established binding partners of the FBM of Crb, Ex and Yrt (Ling et al., 2010; Robinson et al., 2010; Laprise et al., 2006), mediates the Crb function in the AS. So far, no role of Ex during DC has been reported, and *ex* mutant embryos reach stage 16 of development without showing major morphogenetic defects (Marcinkevicius and Zallen, 2013). Yrt is expressed in the AS and the epidermis, but this is not affected in $foscrb_{Y10A}$ embryos. In addition, the DC phenotype of zygotic $yrt^{\Delta 75a}$ mutants is less severe than the one observed in $foscrb_{Y10A}$ embryos. Finally, we do not observe increased Crb protein levels in $foscrb_{Y10A}$ embryos, which would be expected if the interaction between Yrt and Crb is impaired (Laprise et al., 2006).

Further support for a more direct role of Crb in regulating the actomyosin network comes from the observation that Crb co-localises with *D*Par-6, aPKC and Baz at the medial actomyosin foci in the AS (David et al., 2010; 2013). Given the known interactions between members of the Crb complex with members of the Par complex [reviewed in (Bulgakova and Knust, 2009; Tepass, 2012; Rodriguez-Boulan and Macara, 2014)], David et al. (David et al., 2010) suggest that Crb in apical medial foci provides an anchor for PAR proteins. They go on to show that Baz and Par6-aPKC have opposite effects on foci duration, in that Baz promotes and Par6-aPKC complex inhibits the duration of foci. The interplay between these polarity complexes and the actomyosin system seems to establish a delayed negative feedback that promotes the cyclic contractions in the AS (David et al., 2010; 2013). In fact, Crb::GFP also exhibits a similar pulsation as Zip::GFP in the AS (own unpublished observations), so it will be important to analyse whether Crb_{Y10A}::GFP mutant proteins have different dynamics in comparison to the wild type Crb.

Crb –a regulator of ZA integrity via actomyosin dynamics?

Given the observation that at early stages of embryonic development the PBM is required for ZA stability, and that the Crb_{Y10A} mutant protein has an intact PBM, it is possible that during DC, Crb-mediated regulation of actomyosin dynamics impacts on ZA stability. Interestingly, *D*Pak is not only a regulator of actomyosin dynamics, but is also involved in supporting ZA stability, both in *Drosophila* and in mammalian cells (Lozano et al., 2008; Braga et al., 2000; Akhtar and Hotchin, 2001; Pirraglia et al., 2010; Menzel et al., 2008; 2007). The role of *D*Pak itself in DC morphogenesis is still controversial. Previous work showed that cell shape changes in

the AS occur normally in embryos lacking maternal and zygotic *Dpak* and that inhibition of *D*Pak in the AS does not prevent apical constriction of amnioserosa cells (Conder et al., 2004). However, wild-type embryos expressing Pak-AID in the AS show defects in head involution and DC, which are stronger than those of embryos devoid of maternal and zygotic *D*Pak. This led the authors to suggest that Pak-AID may also affect the activity of a second kinase, Pak3, in the AS (Conder et al., 2004). Thus, whether inhibition of *D*Pak, Pak3 or both upon expression of Pak-AID in $foscrb_{Y10A}$ embryos accounts for the rescuing effect of the DC phenotype, including rescue of the ZA, remains to be clarified.

How can *D*Pak regulate ZA integrity? ZA remodelling is essential for morphogenesis, and this remodelling is driven by the endocytosis and recycling of junctional components (Harris, 2012; Matsubayashi et al., 2015). *D*Pak can activate the Arp2/3 complex directly or via the *Drosophila* WAVE homolog SCAR (Lecuit et al., 2011; Kurisu and Takenawa, 2009; Zallen et al., 2002). Arp2/3, in turn, has been implicated in the regulation of ZA stability, e.g. in the *Drosophila* notum, where it maintains ZA stability by regulating the endocytosis of junctional components (Watanabe et al., 2009; Quiros and Nusrat, 2014; Lecuit et al., 2011; Georgiou et al., 2008; Leibfried et al., 2008). Moreover, reducing the activity of the Arp2/3-complex suppresses the DC phenotype of *α-Cat* mutants (Sarpal et al., 2012), and the Arp2/3–WAVE/SCAR complexes associate with E-cad clusters and regulate their endocytosis (Verma et al., 2012; Kovacs et al., 2002; Lecuit and Yap, 2015). In fact, *D*E-cad endocytosis is enhanced in a Rho1-dependent manner when junctions are under stress and *D*E-cad clusters are also down-regulated via inhibition of Par3 by Rok (Levayer et al., 2011; Lecuit and Yap, 2015). Our results are in agreement with a role of Arp2/3 in regulating ZA stability in the AS. Heterozygosity of $SCAR^{\Delta 37}$, $Arp1^{Q25st}$ or $Arp3^{EP3640}$ not only partially restored *D*E-cad::GFP localisation at the ZA in the AS of $foscrb_{Y10A}$ embryos and suppressed DC defects, but even rescued the lethality of $foscrb_{Y10A}$ flies. Fusion of abdominal segments in adult escapers suggest that Crb may also be involved in histoblast fusion during metamorphosis (Madhavan and Madhavan, 1980; Ninov et al., 2007). Myosin-II activity itself has also been shown to be essential for the maintenance of AJs in some cases. Mice ablated for NMHC II-A die by E7.5 due to massive defects in cell-cell contacts and epithelial multi-layering accompanied by loss of E-cad and β-catenin from adhesion sites (Conti et al., 2004). Similarly, ZA stability in the *Drosophila* embryonic ectoderm depends on myosin-II contractility and requires interactions with actin (Engl et al., 2014; Truong Quang et al., 2013). Finally, Rok and myosin-II activities participate in ZA remodelling in the *Drosophila* pupal eye by regulating the formation of *D*E-cad recycling endosomes (Yashiro et al., 2014). Because the SCAR-Arp2/3 complex is an important enhancer of actin protrusions (Wood et al., 2002; Abreu-Blanco et al., 2012; Georgiou and Baum, 2010), it is also plausible that reducing its activity in $foscrb_{Y10A}$ embryos stabilises the ZA indirectly.

On the other hand, misregulation of actomyosin activity is not always associated with defects in ZA stability and integrity of the AS. Expressing a constitutively active form of MLCK to increase myosin II activity or over-expression of RhoGEF2, an activator of Rho1, results in an increase in the number and density of actin foci without affecting the integrity of the AS (Azevedo et al., 2011; Fischer et al., 2014), which could be due to the use of a weak GAL4 driver. Alternatively, the difference to our results could be explained by the fact that these authors performed the over-expression in a background with more than two copies of E-cad (using a ubi-*D*E-cad::GFP line), while we performed the experiments in a knock-in *D*E-cad::GFP line (Huang et al., 2009; 2011), which thus may represent a more sensitive background.

Crb –an organiser of a platform to link the ZA with the actomyosin network?

Another possibility to interpret our results is that Crb, or an interacting protein, couples the actomyosin network and the ZA. During gastrulation in *C. elegans* a molecular clutch has been postulated to connect the myosin network with the adhesion sites to transmit the force generated by the actomyosin contractions (Roh-Johnson et al., 2012). In *Drosophila*, the actomyosin contractions in the AS are initially uncoupled from apical contractions and hence the ZA (Solon et al., 2009; Gorfinkiel et al., 2009; Blanchard et al., 2010). Successive rows of amnioserosa cells are then sequentially stabilised in a contracted state, driving further contraction of the tissue. The surface stabilization mechanism is not known, but is likely to involve an increase in cellular stiffness [reviewed in (Paluch and Heisenberg, 2009)]. In $foscrb_{Y10A}$ embryos the actomyosin foci in the AS emerge prematurely before the onset of germ band retraction, whereas in wild-type these foci are more abundant after the end of germ band retraction (Figure 2-figure supplement 2 and data not shown). Thus, the early over-contraction of the actomyosin in $foscrb_{Y10A}$ embryos may induce a premature coupling to the ZA, thus disrupting germ band retraction and DC. An interesting candidate for this coupling is the protein Canoe, which binds to α-catenin (Sawyer et al., 2009; Pokutta et al., 2002), and whose absence results in a DC phenotype (Jürgens et al., 1984; Takahashi et al., 1998; Boettner et al., 2003; Choi et al., 2011). Absence of Canoe induces the detachment of the actomyosin apparatus from cell-cell junctions during *Drosophila* mesoderm invagination (Sawyer et al., 2009; 2011).

In conclusion, we show a novel function of the FBM of Crb as an essential regulator of cytoskeleton dynamics and tissue integrity during DC. Different lines of evidence show that Crb regulation of AS morphogenesis involves *D*Moesin, Rho-GTPases, class-I Pak, and the SCAR-Arp2/3 complex. Further work will determine at which level Crb regulates actomyosin dynamics and why it is just the morphogenesis of the AS that depends on the FBM of Crb, while all other embryonic epithelia are not affected.

Materials and Methods

Fly stocks (see Table 1)

Flies were maintained at 25ºC on standard food. All the mutant alleles where balanced over fluorescent balancers to identify the homozygous mutants in fixed embryos or live imaging microscopy (see below). All crosses and analyses were carried in a *crb* null background (crb^{GX24} or crb^{11A22}, homozygous or trans-heterozygous), so the expression of the different variants of Crb is exclusively provided by the fosmid (Klose et al., 2013). The different UAS-lines where recombined with the *D*E-cad::GFP knock-in allele or the null crb^{11A22} allele. The driver line $GAL4^{332.3}$ was recombined with each of the different fosmid alleles.

Embryo collection and antibody staining

Embryo stage refers to the $foscrb;crb^{GX24}$ genotype morphology accordingly to (Campos-Ortega and Hartenstein, 1985). All genotypes ($foscrb;crb^{GX24}$, $foscrb_{Y10F};crb^{GX24}$ and $foscrb_{Y10A};crb^{GX24}$) were collected under the same conditions, at the same time and during the same period (indicated in the respective figure legend). In this way, the comparison between *foscrb* or $foscrb_{Y10F}$ and $foscrb_{Y10A}$ mutant phenotypes show the differences observed at a specific time after egg laying. Embryos were collected on apple juice plates at 25ºC and then incubated for the appropriate times at 25ºC or 28ºC, dechorionated in 3% sodium hypochlorite for 3 min, fixed for 20 min in 4% formaldehyde in phosphate-buffered saline (PBS) solution/heptane V/V 1:1. Vitelline membrane was removed by strong shaking in heptane/methanol v/v 1:1, except for the staining of actin in which the vitelline membrane was removed by strong shaking in 80% ethanol. Embryos were blocked for 2 hr at room temperature in PBT (PBS + 0.1% Triton X-100) + 5% normal horse serum (Sigma-Aldrich H1270, St. Louis, Missouri, USA). Embryos were incubated for 2 hr at room temperature or overnight at 4ºC with primary antibodies (see Table 2). For analysis of Zipper localisation, we used the protein trap line *Zipper::GFP* (see Table 1) and the staining was done using the anti-GFP antibody. Incubations with the appropriate secondary antibodies were performed for 1 hr at room temperature. Stained embryos were mounted in glycerin propyl gallate (75% glycerol, 50 mg/mL propyl gallate) and visualized using a Zeiss LSM 780 NLO confocal microscope (ZEISS Microscopy, Jena, Germany) with a C-Apochromat 40x/1.2W Corr objective with the correction collar at 0.18 (at this position the brightness and contrast was enhanced). To distinguish homozygous embryos, in all the stainings an anti-GFP antibody was included to stain for the balancer-provided GFP. All images for a given marker in different genotypes were taken under the same settings for laser power, PMT gain and offset. Maximal projections, merging and LUT-pseudocolor assignment was performed using Fiji (Schindelin et al., 2012). For the FIRE-LUT pseudocolor 0 is black and 255 is white. Mounting was done in Adobe Photoshop CC 2015.0.1 and when brightness and contrast was adjusted, the modifications were equally applied to all the set of images for a given marker.

Cuticle preparation

598 Embryos were collected overnight on apple juice plates at 25ºC and then incubated for > 6 h at 28ºC. All the
599 GFP or YFP positive eggs (the GFP or YFP is provided by the balancer) were removed and the remaining eggs
600 where maintained at 25ºC. The next day, the plates were screened again to remove remaining GFP/YFP positive
601 eggs/larvae. Thus, all the remaining eggs/larvae had a *crb* null background (crb^{GX24} or crb^{11A22}, homozygous or
602 trans-heterozygous). These eggs/larvae were collected, dechorionated in 3% sodium hypochlorite for 3 min,
603 mounted on Hoyer's medium (gum arabic 30 g, chloral hydrate 200 g, glycerol 20 g, H_2O 50 ml), and the slide
604 was incubated overnight at 60ºC. In this way, all the eggs laid in the plate were at least >28 h at 25º, enough time
605 to let the larvae hatch when they are viable. The preparations were analysed by phase contrast with a Zeiss Axio
606 Imager.Z1 microscope with an EC Plan-NEOFLUAR 10X/0.3 objective.

607 **Scanning electron microscopy (SEM)**

608 Embryos were collected on apple juice plates for 1 hr at 25ºC and then incubated for 8 h at 28ºC, dechorionated
609 in 3% sodium hypochlorite for 2 min 30 sec, and fixed for 30 min in 25% glutaraldehyde/heptane v/v 1:1.
610 Devitellinization was done by hand in 25% glutaraldehyde. Then, the embryos were postfixed in modified
611 Karnovsky (2% paraformaldehyde/2% glutaraldehyde in 50 mM HEPES) followed by 1% osmium tetroxide in
612 PBS, dehydrated in a graded series of ethanol, transferred to microporous capsules (78 µm pore size, Plano Cat.
613 4614) and critical point dried using the Leica CPD 300 (Leica Microsystems GmbH, Wetzlar, Germany).
614 Embryos were mounted on 12 mm aluminium stubs and sputter coated with gold using a Leica Baltec SCD 050.
615 Samples were analysed with a Jeol JSM 7500F cold field emission SEM (JEOL Ltd, Tokyo, Japan) at 10 kV
616 acceleration voltage.

617 **Live imaging**

618 Embryos were collected and incubated as describe above (see **Embryo collection and antibody staining)**. In
619 the analysis of pulsed contractions in the AS, sequential collections of 30 min interspaced by 1 hr between each
620 genotype allowed us to analyse 2-3 embryos of each genotype on the same session, so the acquisition conditions
621 for all the genotypes were identical. To eliminate crb^{GX24} or crb^{11A22} heterozygous embryos, all GFP or YFP
622 positive embryos were removed. The remaining eggs were dechorionated by hand or in 3% sodium hypochlorite
623 for 2 min, mounted and oriented in a bottom glass Petri dish (MatTek P35G-1.5.14-C, Ashland, Massachusetts,
624 USA). Previously, the glass was cover with a thin layer of glue (adhesive dissolved from double sided tape in
625 heptane). The embryos were covered with water and visualized by multi-position scanning using a Zeiss LSM
626 780 NLO confocal microscope with a W Plan-Apochromat 40x/1.0 objective. Excitation was performed with
627 488 nm for GFP or YFP, and 561 nm for RFP or mTomato from an Argon Multiline Laser. The pinhole was
628 adjusted for faster acquisition, so the step sizes correspond to 2.01 µm (Videos 1, 2, 7, 11, 13, 14), 2.3 µm
629 (Videos 4, 5, 6), 1.2 µm (Video 8, 12), 1.46 µm (Videos 3 and 9). 4D-Hyperstacks were processed with Fiji

630 (Schindelin et al., 2012) and the movies were rendered with Adobe Photoshop CC 2015.0.1. Under these
631 conditions we observed that *w;foscrb,DE-cad::GFP;crb*^{GX24} embryos imaged for >7 hr at 5 min time lapse
632 hatched and survived without showing any obvious damage (data not shown).

633 **Statistical analyses**

634 Statistical analyses were performed with GraphPad Prism 6. Results are expressed as means ± SD. Statistical
635 significance was evaluated in a one-way analysis of variance (ANOVA) followed by a Dunnett's multiple-
636 comparison test. In the analysis of the statistical significance of the data presented in the Figure 7-figure
637 supplement 1, the percentages were first converted to arcsin values and then analysed by a one-way-ANOVA
638 followed by a Dunnet's multiple comparisons test.

639

640

641

642 Table 1. List of fly stocks used in this study

Fly stock	Description
w	All stocks have the *w** or w^{1118} background
w;foscrb *w;foscrb*$_{Y10F}$ *w;foscrb*$_{Y10A}$	Flies expressing fosmid variants of crb under the control of the endogenous promoter and inserted into the landing site *attP40* on 2nd chromosome; described in (Klose et al., 2013)
w;;crb^{11A22}*/TTG*	*crb* null allele; BSC 3448
w;;crb^{GX24}*/TTG*	*crb* null allele (Huang et al., 2009)
w;;yrt$^{\Delta 75a}$*crb*^{11A22}*/TTG*	*yrt* protein null allele recombined with the *crb*^{11A22} allele (Laprise et al., 2006)
w;;puc^{E69}*/TTG*	lacZ enhancer trap in the *puc* locus, a read-out of JNK signalling (Ring and Martinez Arias, 1993; Martín-Blanco et al., 1998)
w;SCAR$^{\Delta 37}$*/CTG*	Loss of function allele (Zallen et al., 2002); BSC 8754
w;;Arp3^{EP3640}*/TTG*	generated by Berkeley *Drosophila* Genome Project (Hudson and Cooley, 2002); BSC 17149
w;ex^{697}*/CTG*	lacZ enhancer trap in the *ex* locus; kindly provided by Nick Tapon
w;nub^{1}*Arpc1*^{Q25st} *FRT40A/CTG*	Nonsense mutation at Gln25 (CAG→TAG); behaves as a null mutant (Hudson and Cooley, 2002); BSC 9135
w flw^{6}*/FTG*	Amorphic allele (Raghavan et al., 2000); BSC 23693
y w rok^{2} *FRT19A/FTG*	Encodes the first 21 amino acids of rok followed by a 35 aa random peptide and a stop codon (Winter et al., 2001); BSC 6666
w;Rho1^{1B}*/CTG*	*Rho1* loss of function allele; BSC 9477
w;DE-cad::GFP	DE-cadherin fused with GFP knock-in allele; homozygous viable (Huang et al., 2009)
w;DE-cad::mTomato	DE-cadherin fused with mTomato knock-in allele; homozygous viable (Huang et al., 2009)
w;Zipper::GFP	Protein trap line: Zipper fused with GFP under endogenous promoter; homozygous viable; BSC 51564.
w;sqh::Utrophin::GFP	Actin binding domain of human Utrophin fused with GFP under the control of the *sqh* promoter (Rauzi et al., 2010).
w;;Sas::Venus	On 3rd; Stranded at Second fused with Venus under tubulin promoter (Firmino et al., 2013)
w; GAL4$^{332.2}$	On 2nd; expresses GAL4 in amnioserosa; BSC 5398
w; UAS-Apoliner	On 2nd; engineered apoptotic reporter (Bardet et al., 2008); BSC 32122
w; UAS-flw-HA	On 2nd; HA-tagged flw protein under UAS control; BSC 23703
w;; UAS-Rho1^{N19}	On 3rd; dominant negative Rho1 under the control of UAS; BSC 7328
w;; UAS-Rac^{N17}	On 3rd; dominant negative Rac under the control of UAS; BSC 6292
w; UAS-Cdc47^{N17}	On 2nd; negative Cdc42 under the control of UAS; BSC 6288. The stock *w;DE-cad::GFP,UAS-Cdc42*^{N17}*/(CTG);crb*^{11A22}*,UAS-Actin::RFP/TM6B-YFP* or *TTG* was not possible to obtain, probably because the expression of Cdc^{N17}, induced by the GAL4 from the balancer chromosome is detrimental.
w;; UAS-moe^{T559D}*-myc*	On 2rd; phosphomimetic Moesin under the control of UAS; BSC 8630
w;; UAS-moe-myc	On 3rd; myc-tagged Moesin under the control of UAS; BSC 52236
w; UAS-Pak-myr	On 2nd: constitutively-active, membrane-bound Pak under UAS control; BSC 8804
w; UAS-Pak-AID	On 2nd; Pak autoinhibitory domain under UAS control; kindly provided by Nicholas Harden (Conder et al., 2004)
w;; UAS-Act::RFP	On 3rd; RFP-tagged Act5C under UAS control; BSC 24779
w;; UAS-rok-CAT-KG	On 3rd; a kinase-dead rok under UAS control; BSC 6671
FTG	Balancer on 1st *FM7c, twi-GAL4 UAS-EGFP*; from BSC 6873
CTG	Balancer on 2nd *CyO, twi-GAL4 UAS-EGFP*; from BSC 6662
TTG	Balancer on 3rd *TM3, twi-GAL4 UAS-EGFP Sb*^{1} *Ser*^{1}; from BSC 6663
TM6B-YFP	Balancer on 3rd *TM6B, Dfd-EYFP, Sb*^{1} *Tb*^{1} *ca*^{1}; from BSC 8704

643 BSC - Bloomington stock center; DGRC - Drosophila Genetic Resource Center.

644

645 Table 2. Antibodies and probes employed
646

	Dilution	Source
Phalloidin Alexa Fluor 555	1:500	Invitrogen
Alexa Fluor 488-, 568-, and 647-conjugated	1:500	Invitrogen
Rat antibodies		
anti-Crb2.8	1:500	(Richard et al., 2006)
anti-*D*E-cadherin	1:20	DSHB DCAD2
anti-Yurt	1:100	(Laprise et al., 2006)
Mouse antibodies		
anti-α-Spectrin	1:25	DSHB 3A9
anti-β-galactosidase	1:200	DSHB 40-1a
anti-Coracle	1:25	DSHB C566.9
anti-Crb-Cq4	1:300	DSHB Cq4
anti-Disc large	1:100	DSHB 4F3
anti-Enabled	1:100	DSHB 5G2
anti-GFP	1:500	Roche 11814460001 (Mannheim, Germany)
anti-Hindsight	1:100	DSHB 1G9
anti-Integrin β_{PS}	1:2	DSHB CF.6G11
anti-Phosphotyrosine	1:100	BD Transduction Laboratories cat. no. 610000
anti-SCAR	1:25	DSHB P1C1
Rabbit antibodies		
anti-Bazooka	1:500	kindly provided by A. Wodarz
anti-DAAM	1:3000	kindly provided by József Mihály (unpublished)
anti-Diaphanous	1:5000	kindly provided by Steven A. Wasserman (Afshar et al., 2000)
anti-*D*Patj	1:1000	(Richard et al., 2006)
anti-Echinoid	1:5000	kindly provided by Laura Nilson (Laplante and Nilson, 2006)
anti-Expanded	1:300	(Boedigheimer and Laughon, 1993)
anti-GFP	1:500	Invitrogen
anti-*D*Pak	1:8000	kindly provided by Nicholas Harden (Harden et al., 1996)
anti-Polychaetoid	1:5000	kindly provided by Sarah Bray (Djiane et al., 2011)
anti-Phospho-Moesin	1:100	Cell Signaling Technology 3150 (Danvers, Massachusetts, USA)
anti-Stranded at second	1:500	kindly provided by E. Organ and D. Cavener

647
648 Invitrogen, Molecular Probes (Eugene, Oregon, USA); DSHB - Developmental Studies Hybridoma Bank (Iowa
649 city, Iowa, USA)
650

Table 3. Statistical analyses of the results shown in the Figure 7-figure supplement 1.

			Open cuticle	Dorsal hole	Closed but not hatched	Kinked larvae	WT-like
	1	*foscrb$_{Y10A}$;crb^{GX24}*					
vs	14	*foscrb$_{Y10A}$/Rho1^{1B};crb^{GX24}*	**	ns	ns	*	***
	2	*foscrb$_{Y10A}$,DE-cad::GFP;crb^{GX24}*					
vs	23	*foscrb$_{Y10A}$,DE-cad::GFP/SCAR$^{\Delta 37}$,DE-cad::GFP;crb^{GX24}*	****	ns	ns	****	****
vs	25	*foscrb$_{Y10A}$,DE-cad::GFP/Arpc^{1Q25st},DE-cad::GFP;crb^{GX24}*	ns	ns	ns	ns	ns
	3	*foscrb$_{Y10A}$,DE-cad::GFP/+;crb^{11A22}/crb^{GX24}*					
vs	11	*flw^{6}/Y/w*;foscrb$_{Y10A}$,DE-cad::GFP/+;crb^{11A22}/crb^{GX24}*	****	**	**	ns	ns
vs	15	*rok^{2}/Y/w*;foscrb$_{Y10A}$,DE-cad::GFP/+;crb^{11A22}/crb^{GX24}*	*	ns	ns	ns	ns
vs	24	*foscrb$_{Y10A}$,DE-cad::GFP/+;crb^{11A22},Arp3^{EP3640}/crb^{GX24}*	ns	ns	ns	ns	**
	5	*foscrb$_{Y10A}$,GAL4$^{332.3}$/DE-cad::GFP;crb^{GX24}/crb^{11A22}*					
vs	7	*29ºC foscrb$_{Y10A}$,GAL4$^{332.3}$/UAS-Crb$^{full\ length}$;crb^{GX24}/crb^{11A22}*	ns	ns	ns	ns	ns
vs	8	*25ºC foscrb$_{Y10A}$,GAL4$^{332.3}$/UAS-Crb$^{full\ length}$;crb^{GX24}/crb^{11A23}*	ns	ns	ns	ns	****
vs	9	*18ºC foscrb$_{Y10A}$,GAL4$^{332.3}$/UAS-Crb$^{full\ length}$;crb^{GX24}/crb^{11A24}*	ns	ns	ns	ns	****
vs	12	*foscrb$_{Y10A}$,GAL4$^{332.3}$/DE-cad::GFP;crb^{GX24}/crb^{11A22},UAS-Rho^{N19}*	**	ns	ns	ns	**
vs	13	*foscrb$_{Y10A}$,GAL4$^{332.3}$/DE-cad::GFP;crb^{GX24}/crb^{11A22},UAS-rok.CAT-KG*	ns	ns	ns	ns	*
vs	16	*foscrb$_{Y10A}$,GAL4$^{332.3}$/DE-cad::GFP;crb^{GX24}/crb^{11A22},UAS-Rac^{N17}*	ns	ns	ns	ns	ns
vs	21	*foscrb$_{Y10A}$,GAL4$^{332.3}$/DE-cad::GFP;crb^{GX24}/crb^{11A22},UAS-Dmoe-myc*	ns	ns	ns	ns	ns
vs	22	*foscrb$_{Y10A}$,GAL4$^{332.3}$/UAS-DE-cad,DE-cad::GFP;crb^{GX24}/crb^{11A22}*	****	***	ns	ns	****
	6	*foscrb$_{Y10A}$,GAL4$^{332.3}$/DE-cad::GFP;crb^{GX24}/crb^{11A22},UAS-Act::RFP*					
vs	10	*foscrb$_{Y10A}$,GAL4$^{332.3}$/UAS-flw-HA,DE-cad::GFP;crb^{GX24}/crb^{11A22},UAS-Act::RFP*	ns	****	ns	*	****
vs	17	*foscrb$_{Y10A}$,GAL4$^{332.3}$/UAS-DPak-AID,DE-cad::GFP;crb^{GX24}/crb^{11A22},UAS-Act::RFP*	ns	****	ns	ns	****
vs	20	*foscrb$_{Y10A}$,GAL4$^{332.3}$/UAS-Dmoe^{T559D},DE-cad::GFP;crb^{GX24}/crb^{11A22},UAS-Act::RFP*	ns	*	ns	ns	****
	18	*foscrb,GAL4$^{332.3}$/UAS-Dpak-myr,DE-cad::GFP;crb^{GX24}/crb^{11A22},UAS-Act::RFP*					
vs	19	*foscrb,GAL4$^{332.3}$/DE-cad::GFP;crb^{GX24}/crb^{11A22},UAS-Act::RFP*	**	***	****	ns	****

One-way-ANOVA analysis followed by a Dunnet's multiple comparisons test between the indicated categories of the different genotypes. Statistical significant difference indicated as follows: **ns** $P > 0.05$; * $P \leq 0.05$; ** $P \leq 0.01$; *** $P \leq 0.001$; **** $P \leq 0.0001$.

Acknowledgments

Stocks obtained from the Bloomington Drosophila Stock Center (NIH P40OD018537) were used in this study. Antibodies obtained from the Developmental Studies Hybridoma Bank, created by the NICHD of the NIH and maintained at The University of Iowa, Department of Biology, Iowa City, IA 52242.

We thank Thomas Kurth (Biotec Dresden) for the scanning electron microscopy analysis and the LMF facility of MPI-CBG for microscopy support. We thank Sarita Hebbar and Johanna Lattner for critical reading of the manuscript, and Perla Zerial for her advice on the statistical analysis. The work was supported by funding from the Max-Planck Society.

FIGURE LEGENDS

Figure 1. **The FERM-binding domain motif (FBM) of Crb is essential for dorsal closure (DC)**.

(**A-F**) Stills from dorsal views of live imaging of embryos expressing *D*E-cad::GFP. In all images the anterior part is towards the left. A, C and E, *w;foscrb,DE-cad::GFP;crb^{GX24}* (Video 1). B, D and F, *w;foscrb$_{Y10A}$,DE-cad::GFP;crb^{GX24}* (Video 2). All embryos were collected at the same time (1 h collection), incubated at 28ºC for 7 h and imaged together. Numbers in (B,D and F) indicate the time in minutes for the corresponding row. While DC is completed in *foscrb* embryos (E), in *foscrb$_{Y10A}$* embryos, the amnioserosa (AS) is disorganised and progressively lost (F). Scale bar: 100 µm. (**G-J'**) Localisation of phosphotyrosine (PY), Crb and *D*Patj in the dorsal epidermis at the beginning of DC. In all images the AS is at the top (see reference axis in G and in the scheme I). (G, I-I') *w;foscrb;crb^{GX24}*. (H, J-J') *w;foscrb$_{Y10A}$;crb^{GX24}*. (**K**) Schematic representation of the dorsal epidermis at the beginning of DC indicating that the leading edge (LE) of the dorsal most epidermal (DME) cells is in contact with the AS. Arrows in (G,H) indicate LE of the DME (row of cells marked by brackets). The arrowheads indicate where the corresponding protein is absent from the LE (I-J'). The asterisks mark LE membranes positive for Crb (J) and *D*Patj (J') in *foscrb$_{Y10A}$* mutant. Scale bar: 10 µm. Representative images from 8-12 different embryos for each genotype.

Figure 1-figure supplement 1. **DC in *foscrb$_{Y10F}$* embryos**.

(**A-C**) Stills from dorsal views of live imaging of embryos expressing *D*E-cad::GFP in *w;foscrb$_{Y10F}$,DE-cad::GFP;crb^{GX24}*. Embryos collected and imaged as described in Figure 1. Numbers indicate the time in minutes for the corresponding row. DC proceeds as in *foscrb* embryos. Scale bar: 100 µm.

Figure 2. **The FBM of Crb is important the establishment of the supracellular actomyosin cable at the LE of the DME cells during DC**.

(**A-L**) Localisation of Stranded at second (Sas, A,B), Enabled (Ena, C,D), Actin (E,F), Zipper (Zip, E',F'), Echinoid (Ed, G,H), phosphotyrosine (PY, G',H'), Bazooka (Baz, I,J), and *D*E-cadherin (*D*E-cad, K,L) at the beginning of stage 14. In all images the AS is at the top half, for the genotypes *w;foscrb;crb^{GX24}* and *w;foscrb$_{Y10A}$;crb^{GX24}*. Filopodia extend dorsally in *foscrb* embryos (A, arrow), but in *foscrb$_{Y10A}$* embryos filopodia are absent (B, arrowhead) or disorganised (B, empty arrowhead). Ena, Actin and Zip concentrate at the LE in *foscrb* embryos (C,E and E', arrows), but these proteins are almost absent from the LE in *foscrb$_{Y10A}$* embryos (D,F and F', arrowheads). Ed is absent from the LE of *foscrb* embryos (G, arrowhead), but the DME cells of *foscrb$_{Y10A}$* embryos show an important decrease of the protein (H, magenta overlay) though the PY staining is

still clearly associated with the ZA in the same cells (H', magenta overlay). Similarly, Baz decreases at the LE of *foscrb* embryos (I, arrowhead), but in *foscrb*$_{Y10A}$ embryos, the cells that do not elongate keep Baz at the LE (J, arrow), while other DME cells show a reduction of Baz (J, and Figure 2-figure supplement 3). *D*E-cad (mTomato signal) localises at all cell-cell contacts in *foscrb* embryos (K). However, in *foscrb*$_{Y10A}$, the *D*E-cad localisation is affected in both the dorsal epidermis (L, solid arrowhead) and the AS (L, empty arrowheads). Scale bar: 10 µm. **(M)** Schematic representation of the changes in DME cells at the beginning of DC in embryos expressing either fosCrb or fosCrb$_{Y10F}$. The elongation of the DME cells is accompanied by the removal of the Crb protein complex, Ed, Baz and the septate junction components from the LE. At the LE a supracellular actomyosin cable is established and filopodia extend dorsally and attach to the AS cells. Representative images from 8-12 different embryos for each genotype. (**N**) Schematic representation of the defects in the DME cells of embryos expressing the fosCrb$_{Y10A}$ variant. At the beginning of DC, the DME cells do not elongate uniformly. In the cells that do not elongate, the Crb protein complex and Baz remain at the LE. Reduced *D*E-cad suggest defects in the ZA function. Ed is dramatically reduced in DME cells, probably contributing to the absence of the supracellular actomyosin cable. Also, the DME cells exhibit disorganised filopodia. Nevertheless, the septate junction components are properly removed from the LE. The Crb protein complex is apical to the ZA, but Ed and the actomyosin cable are associated with the ZA.

Figure 2-figure supplement 1. **Localisation of Pyd, Dia and DAAM in *foscrb* and *foscrb*$_{Y10F}$ embryos**.
Localisation of Polychaetoid (Pyd, **A,B**), Phosphotyrosine (PY, **A',B'**), Diaphanous (Dia, **C,D**), and Dishevelled Associated Activator of Morphogenesis (DAAM, **E,F**) in embryos at the beginning of stage 14. In all images the AS is at the top, for the genotypes *w;foscrb;crb*^{GX24}, and *w;foscrb*$_{Y10A}$*;crb*^{GX24}. The localisation of Pyd (A-B'') is comparable between the different genotypes, despite the irregularly extended DME cells in *w;foscrb*$_{Y10A}$*;crb*^{GX24} embryos (B,B',B''). The PY staining (A',B') marks the ZA. The localisation of Dia (C,D) and DAAM (E,F) is similar in the different genotypes. Scale bar: 10 µm. Representative images from 8-12 different embryos for each genotype.

Figure 2-figure supplement 2. **The FBM of Crb is important for the establishment of the supracellular actomyosin cable**.
Stills from live imaging of embryos expressing Zip::GFP. In all images the anterior part is to the left. (**A-C**) *w;foscrb/Zip::GFP;crb*^{GX24} and (**D-F**) *w;foscrb*$_{Y10A}$*/Zip::GFP;crb*^{GX24} embryos were followed during GB retraction. Numbers in (D-F) indicate the time in minutes for the corresponding row. Arrow in (B) marks the incipient formation of the supracellular actomyosin cable in a *foscrb* embryo. The supracellular actomyosin

cable is continuous at later time points (C, arrow). In *foscrb*$_{Y10A}$ embryos, some segments of the DME cells concentrate Zip::GFP at the LE (E, arrow). At the time when GB retraction should be completed and thereafter, the actomyosin cable forms randomly at the LE (F, arrows), and several discontinuities are present (F, arrowheads). Scale bar: 100 µm. Representative images from 6-8 different embryos for each genotype.

Figure 2-figure supplement 3. **Reduction of Baz in DME cells of *foscrb*$_{Y10A}$ embryos**.

Localisation of Bazooka (Baz, **A,B**), and phosphotyrosine (PY, **A',B'**) at the beginning of stage 14 in *w;foscrb;crb*^{GX24} and *w;foscrb*$_{Y10A}$*;crb*^{GX24} embryos. The black lines in A-B' mark the position for the plot profile (**C,D**) of the Baz signal (C,D, black line) and the PY signal (C,D, magenta line) in the DME cells. Maxima intensities overlap for both markers, but note that the intensity of Baz in *foscrb*$_{Y10A}$ embryos is lower than in *foscrb* embryos. The arrows indicate where Baz is preserved at the LE of those cells that do not elongate properly, while the asterisks mark the DME cells that extend normally, and have a reduction of Baz signal in the junctions. Scale bar: 10 µm.

Figure 2-figure supplement 4. **Distribution of septate junction components in DME cells**.

Localisation of Coracle (Cora, **A,B**), *D*E-cad (**A',B'**), Disc large (Dlg, **C,D**) and Yurt (Yrt, **E,F**) in embryos at the beginning of stage 14. In all images the AS is at the top, for *w;foscrb;crb*^{GX24} and *w;foscrb*$_{Y10A}$*;crb*^{GX24} embryos. The septate junction proteins Cora (A,B), Dlg (C,D) and Yrt (E,F) are absent from the LE in all genotypes (arrowheads). Bracket in (B) marks bunching of dorsal epidermis observed in *foscrb*$_{Y10A}$ embryos. The *D*E-cad staining (A',B'), is a maximal projection of the first ~1.5 µm from the surface of the embryo, while the Cora staining is a maximal projection of the whole *Z*-stack. The merge of these projections (A''-B'') shows that Cora is mainly present in the epidermis. Scale bar: 10 µm. Representative images from 8-12 different embryos for each genotype.

Figure 2-figure supplement 5. **Distribution of actomyosin and junctional components in DME cells of *foscrb*$_{Y10F}$ embryos**.

(**A-K**) Localisation of Sas at the filopodia (A, arrow). Ena (B), Actin (C), and Zip (C') concentrate at the LE (arrows). Ed (D, and PY, D'), and Baz (E) are absent from the LE (arrowheads). *D*E-cad::mTomato (F) and Pyd (G, and PY, G') localise at all cell-cell contacts. Localisation of Dia (H) and DAAM (I). The septate junction components Cora (J, the corresponding *D*E-cad, J' and the merge, J''), and Dlg (K) are absent from the LE (J,K, arrowheads). The localisation of all these proteins is similar to the one observed in *foscrb* embryos. Scale bar: 10 µm. Representative images from 8-12 different embryos for each genotype.

Figure 3. **The FBM of Crb is important for the maintenance of the AS**.

(**A-F**) Stills from lateral views of live imaging of *D*E-cad::mTomato knock-in at the beginning of germ band (GB) retraction (Video 4). In all images the anterior part is towards the left, for the genotypes *w;foscrb,DE-cad::mTomato;crb*^{GX24} and *w;foscrb*$_{Y10A}$*,DE-cad::mTomato;crb*^{GX24}. All embryos were collected at the same time (1 h collection), incubated at 28ºC for 5 h and imaged together. The numbers in (D,F) indicate the time in min. for the corresponding row. At stage 11 (A,B,D,E), the AS cells are elongated along the AP-axis, and *D*E-cad::mTomato localises along the ZA (B,E, arrows); in *foscrb*$_{Y10A}$ mutant, the continuity of *D*E-cad::mTomato along the ZA is lost (E, arrowhead) and *D*E-cad::mTomato is also found in large clusters (E, white concave arrowhead). At the end of GB retraction the AS covers the dorsal aspect of *foscrb* embryos (E), but in *foscrb*$_{Y10A}$ (F), GB retraction is impaired and *D*E-cad::mTomato signal is fragmented in the AS (F, arrowheads). Scale bar: 100 µm, except for (B,E) 10 µm.

Figure 3-figure supplement 1. **The FBM of Crb is important for the integrity of the AS**.

(**A-B'**) Scanning electron micrographs of dorsal views of embryos incubated for 8 h at 28ºC after egg collection (1 h collection) for the genotypes *w;foscrb;crb*^{GX24} and *w;foscrb*$_{Y10A}$*;crb*^{GX24}. The boxed area in (A,B) is shown in (A',B') respectively. In *foscrb* embryos (A') the AS appears as a flat continuous monolayer, while in *foscrb*$_{Y10A}$ embryos (B'), the AS is disorganised and some cells exhibit large filopodia (B,B', arrow). Other cells are completely detached and may be AS cells or haemocytes (B,B', arrowheads), and some cells have the appearance of apoptotic cells (B', concave arrowhead). Scale bars: 100 µm (A,B) and 10 µm (A',B'). Representative images from 17-37 embryos for each genotype.

Figure 4. **AS detachment in *foscrb*$_{Y10A}$ embryos is accompanied by premature apoptosis**.

(**A-D**) Stills from dorsal views of live imaging of embryos in which the apoptotic reporter Apoliner is driven in the AS with the line GAL4$^{332.3}$ (Video 6). Apoptotic cells in magenta appear more intense than their neighbours. In all images the anterior part is towards the left for the genotypes *w;foscrb,GAL4*$^{332.3}$*/foscrb,UAS-Apoliner;crb*^{GX24}, and *w;foscrb*$_{Y10A}$*,GAL4*$^{332.3}$*/foscrb*$_{Y10A}$*,UAS-Apoliner;crb*^{GX24}. All embryos were collected at the same time (1 h collection), incubated at 28ºC for 7 h and imaged together. The numbers in (B,D) indicate the time in minutes for the corresponding row. After GB retraction in *foscrb* embryos (A), some apoptotic cells are found mainly at the posterior canthus (A, arrow). In comparison, in *foscrb*$_{Y10A}$ embryos, some of the cells that have detached from the AS (B, arrowheads), as well as those in the posterior edge of the AS (B, arrow), are

apoptotic. As DC is completed in *foscrb* embryos (C), a significant portion of the internalised AS cells are apoptotic, while the remaining internalised cells are still localised in a rod-like structure along the dorsal part of the embryo. In contrast, in $foscrb_{Y10A}$ embryos (D) all the remaining AS cells are apoptotic cells (the GFP signal in (D) does not belong to the AS). Scale bar: 100 μm. Representative images from 8-12 different embryos for each genotype. (**E-K**) Activation of the JNK pathway in the DME cells analysed with the enhancer trap puc^{E69} (β–galactosidase staining). *D*E-cad staining is in green. In all images anterior is to the left for the genotypes *w;foscrb/+;*crb^{GX24}/puc^{E69},crb^{GX24} and *w;*$foscrb_{Y10A}$*/+;*crb^{GX24}/puc^{E69},crb^{GX24}. From the beginning to the end of DC, Puc expression is normally induced on each side of the embryo in the single row of DME cells in both genotypes, and few positive β–gal nuclei appear below the row of DME cells (E,F, arrowheads). In $foscrb_{Y10A}$ embryos at middle DC some β–gal positive cells appear below the DME cells (H, arrowheads). When DC is completed in *foscrb* embryos (I), a single row of cells on each side of the embryo is β–gal positive, even in $foscrb_{Y10A}$ embryos, independently of whether the epidermis contacted the corresponding segment of the epidermis on the dorsal midline (J, dashed line), bunched on the same side of the embryo (J, dotted line) or fail to touch the complementing segment (J, arrow). Scale bar: 10 μm. (**K**) No significant difference in the number of β–gal positive nuclei at middle DC along 50 μm at the dorsal epidermis (indicated by the brackets in G,H), mean±SD, n= 17 embryos per genotype.

Figure 4- figure supplement 1. **Hindsight expression in *foscrb* and $foscrb_{Y10A}$ embryos**.

(**A-D**) Expression of Hindsight (Hnt) at stage 12 (A,C, lateral view) and stage 14 (B,D, dorsal view). In all images the AS is inside the green dotted line. Note that the AS is properly specified in *foscrb* and $foscrb_{Y10A}$ embryos, and at stage 14, Hnt staining is comparable between the two genotypes (B,D), and Hnt is present even in the cells that have detached from the AS in the $foscrb_{Y10A}$ embryos (D, arrowhead). Scale bar: 100 μm.

Figure 4- figure supplement 2. **Localisation of integrin β_{PS} in the AS of *foscrb* and $foscrb_{Y10A}$ embryos**.

(**A,B**) The localisation of the integrin-β_{PS} is similar in *foscrb* and $foscrb_{Y10A}$ embryos. The images are projections of ~1 μm thickness; thus, in some cells it is possible to see the localisation of the integrin-β_{PS} at the basal membrane (arrows), while in other cells it is possible to see the protein localisation at the lateral membrane (arrowheads). The inserts are magnification of a single confocal plane (0.45 μm) through the middle part of the AS cells in the respective genotypes. Scale bars: 10 μm.

Figure 4-figure supplement 3. **Localisation of *D*Patj and Yrt in the dorsal epidermis**.

(**A-C''**) Cross section (*ZX* view –see reference axis in Figure 1I) of the dorsal epidermis of embryos at stage 14 stained for *D*Patj (green) and Yrt (fire LUT-pseudocolor). In all images the apical aspect of the cells is at the top and the dotted line marks the basal aspect. (A-A'') *w;foscrb;crb^{GX24}*. (B-B'') *w;foscrb$_{Y10F}$;crb^{GX24}*. (C-C'') *w;foscrb$_{Y10A}$;crb^{GX24}*. Note that Yrt is concentrated toward the apical aspect of the cells in all genotypes. Scale bar: 5 µm. Representative images from 8-12 different embryos for each genotype.

Figure 4- figure supplement 4. **JNK signalling is normal in *foscrb$_{Y10F}$* embryos**.

(**A-C**) Activation of the JNK pathway in the DME cells analysed with the enhancer trap *puc^{E69}* (β–galactosidase staining). *D*E-cad staining is in green. In all images anterior is to the left. From the beginning to the end of DC, Puc expression is normally induced on each side of the embryo in the single row of DME cells. When DC is completed, a single row of cells on each side of the embryo is β–gal positive (C). Scale bar: 10 µm.

Figure 5. **The FBM of Crb is essential for the regulation of actomyosin activity in the AS**.

Stills from views of the AS in live imaging of embryos expressing *D*E-cad::GFP knock-in (**A,B**, Video 8) or Zip::GFP (**C-D'**, Video 9). In all images the anterior part is towards the left. Scale bar: 10 µm. (A) *w;foscrb,DE-cad::GFP;crb^{GX24}*. (B) *w;foscrb$_{Y10A}$,DE-cad::GFP;crb^{GX24}*. (C) *w;foscrb/Zip::GFP;crb^{GX24}*. (D) *w;foscrb$_{Y10A}$/Zip::GFP;crb^{GX24}*. The embryos were collected during 30 min, incubated at 28ºC for 7 h and imaged under the same conditions. The numbers in (C,D) indicate the time in seconds for the corresponding frame in Video 9. In *foscrb* embryos (A), *D*E-cad::GFP is localised at cell-cell junctions; but in *foscrb$_{Y10A}$* (B) embryos *D*E-cad::GFP continuity is strongly disturbed. (**C',D'**) Kymographs of the Zip::GFP foci in the magenta box in (C,D). Scale bar in (C') 10 sec. (**E**) Histogram of the relative frequency of Zip::GFP foci duration during the pulsed contractions of the AS in *w;foscrb/Zip::GFP;crb^{GX24}*, *w;foscrb$_{Y10F}$/Zip::GFP;crb^{GX24}* and *w;foscrb$_{Y10A}$/Zip::GFP;crb^{GX24}* embryos. The graph in the insert shows all data points collected, and indicates the mean ± SD. ANOVA test followed by a Dunnett's multiple-comparison test; ns-not significant difference. *n* = 150 foci collected from each of the three different embryos.

Figure 5-figure supplement 1. **The FBM of Crb regulates the actomyosin activity in the AS**.

Stills from Video 10 where a Zip::GFP cluster forms and disappears (followed by the bracket) in an AS cell during the pulsed contraction in a *w;foscrb/Zip::GFP;crb^{GX24}* embryo (**A**). In contrast, several Zip::GFP foci are present and do not disappear in the *w;foscrb$_{Y10A}$/Zip::GFP;crb^{GX24}* embryo (**B**). Scale bar: 5 µm.

Figure 6. **Expression of the myosin phosphatase Flapwing in the AS of *foscrb$_{Y10A}$* embryos suppresses the DC defects**.

(**A-F**) Stills from dorsal views of live imaging of embryos expressing *D*E-cad::GFP knock-in and Flw-HA in the AS cells under the control of the GAL4$^{332.3}$ driver (Video 11), for the genotypes *w;foscrb,GAL4$^{332.3}$/UAS-flw-HA,DE-cad::GFP;crb^{GX24}/crb^{11A22},UAS-Act::RFP* and *w;foscrb$_{Y10A}$,GAL4$^{332.3}$/UAS-flw-HA,DE-cad::GFP;crb^{GX24}/crb^{11A22},UAS-Act::RFP*. All embryos were collected at the same time (1 h collection), incubated at 28ºC for 7 h and imaged together. The numbers on (D-F) indicate the time in minutes for the corresponding row. The over-expression of Flw-HA in the AS cells does not produce any obvious phenotype in *foscrb* (A-C) embryos, and it suppresses the DC defects in *foscrb$_{Y10A}$* (D-F) embryos; some defects found include an irregular zippering at the posterior canthus (E, arrow) as well as bunching of the dorsal epidermal (F, bracket). Scale bar: 100 μm. Representative images from 6-9 different embryos for each genotype. (**G**) Scheme of the possible pathways regulated by the FBM of Crb in the AS. Crb: Crumbs; Rok: Rho-kinase; *D*pak: *Drosophila* p21-activated kinase; Flw: Flapwing; *D*MBS: *Drosophila* myosin-binding-subunit; Sqh: spaghetti-squash; Mlck: myosin-light chain kinase.

Figure 6-figure supplement 1. **Normal DC after Flapwing expression in the AS of *foscrb$_{Y10F}$* embryos**.

(**A-C**) Stills from dorsal views of live imaging of embryos expressing *D*E-cad::GFP knock-in and Flw-HA in the AS cells under the control of the GAL4$^{332.3}$ driver, for the genotype *w;foscrb$_{Y10F}$,GAL4$^{332.3}$/UAS-flw-HA,DE-cad::GFP;crb^{GX24}/crb^{11A22},UAS-Act::RFP*. Embryo collection, incubation and imaging as described in Figure 6. The numbers on (A-C) indicate the time in minutes for the corresponding row. The over-expression of Flw-HA in the AS cells does not produce any obvious phenotype. Scale bar: 100 μm. Representative images from 7 different embryos.

Figure 7. **Reduction in actomyosin activity suppresses the DC defects in embryos expressing the *foscrb$_{Y10A}$* variant**.

(**A**) Quantification of the defects observed in cuticle preparations from the genotypes indicated in the graph. For the complete genotype see Figure 7-figure supplement 1. The category "DC defect" includes a range of defects ranging from cuticles of embryos that completed DC but do not hatch, to cuticles with large DC openings. The category "WT-like" includes all larvae that hatch. For details about the classifications see Figure 7-figure supplement 1. Note that all the genotypes have the *foscrb$_{Y10A}$* background, except the ones highlighted in magenta, numbers 18 and 19, that have the *foscrb* background. mean ± SD from 2-4 independent crosses. n = total number of cuticles counted for the indicated genotype. Note that suppression of the DC phenotype in

foscrb$_{Y10A}$ embryos is particularly evident upon expression of Flw-HA (10), Pak-AID (17), and *D*E-cad (22). (**B-F**) Adult flies of the indicated genotypes. In (F), the arrowhead marks the defects in the dorsal abdomen.

Figure 7-figure supplement 1. **Reduction in the actomyosin activity suppresses the DC defects in embryos expressing the *foscrb*$_{Y10A}$ variant**.

Quantification of the defects observed in cuticle preparations from the genotypes indicated in the graph. In the category "Open cuticle", the dorsal opening is so prominent that in some cases the mouthparts are exposed (arrowhead). Category "Dorsal hole" corresponds to those cuticles in which a medium (left picture) or small (right picture) dorsal hole is present, but the anterior part is closed. In the category "Closed but not hatched", the closure is complete, the puckering of the epidermis is noticeable (arrowhead), but the larvae fail to hatch. In the category "Kinked larvae", the puckering of the epidermis (arrowhead) results in larvae with the tail pointing upwards, so the larvae seem to have a kink. In the category "WT-like", no defects are evident so the larvae are alike to wild type. mean ± SD from 2-4 independent crosses. n = total number of cuticles counted for the indicated genotype. For the statistical analysis see Table 3.

Figure 7-figure supplement 2. **Phosphorylated *D*Moesin levels are reduced in embryos expressing the *foscrb*$_{Y10A}$ variant**.

Localisation of phospho-*D*Moesin (P-*D*Moe, **A,B**) in embryos at the beginning of stage 14. In all images the AS is at the top, for the genotypes *w;foscrb;crb*^{GX24} and *w;foscrb*$_{Y10A}$*;crb*^{GX24}. The LE of *foscrb*$_{Y10A}$ embryo is marked with a magenta line (B). Scale bar: 10 µm. Representative images from 9 different embryos for each genotype.

Figure 7-figure supplement 3. **Weak head phenotype of embryos expressing the *foscrb*$_{Y10A}$ variant**.

Examples of cuticles with a weak head phenotype: the arrows mark an opening in the anterior part.

Figure 8. **Reduction of the SCAR-Arp complex activity suppresses the DC defects and ameliorates the loss of *D*E-cadherin in the AS of embryos expressing the *foscrb*$_{Y10A}$ variant**.

(**A-F**) Stills from dorsal views of live imaging of embryos expressing *D*E-cad::GFP knock-in and heterozygous for the *SCAR*$^{\Delta 37}$ loss of function allele (Video 13). In all images the anterior is to the left, for the genotypes *w;foscrb,DE-cad::GFP/SCAR*$^{\Delta 37}$*,DE-cad::GFP;crb*^{GX24} and *w;foscrb*$_{Y10A}$*,DE-cad::GFP/SCAR*$^{\Delta 37}$*,DE-cad::GFP;crb*^{GX24}. All embryos were collected at the same time (1 h collection), incubated at 28ºC for 7 h and imaged together. The numbers in (B,D,F) indicate the time in minutes for the corresponding row. DC occurs

normally in *foscrb* (A,C,D) embryos heterozygous for the $SCAR^{\Delta 37}$ allele, and DC defects are suppressed in $foscrb_{Y10A}$ (B,D,F) embryos; some defects still visible include the impaired GB retraction (compare B with A), asymmetric position of the posterior spiracles (D, arrows), and bunching of the dorsal epidermis (D, bracket). Scale bar: 100 µm. (**G,H**) Magnified views of AS from (A,B, respectively). Note that, in order to make the localisation of *D*E-cad::GFP more perceptible, the autofluorescence of the yolk (visible in A,B) was removed from the original stack by hand using Fiji. Scale bar: 100 µm. Representative images from 6-9 different embryos for each genotype.

VIDEO LEGENDS

Video 1. Dorsal closure (DC) in a *w;foscrb,DE-cad::GFP;*crb^{GX24} embryo. Note that the granules from the yolk are visible because of their strong auto-fluorescence in the green part of the spectrum. Time-lapse: 3.5 min; 12 fps.

Video 2. Defective germ band (GB) retraction and DC phenotype in a *w;*$foscrb_{Y10A}$*,DE-cad::GFP;*crb^{GX24} embryo. Time-lapse: 3.5 min; 12 fps.

Video 3. Filopodia movement at the leading edge (LE) of the dorsal most epidermal (DME) cells in *w;foscrb;*crb^{GX24}*,Sas::Venus* (top) and *w;*$foscrb_{Y10A}$*;*crb^{GX24}*,Sas::Venus* (bottom) embryos. The filopodia at the DME cells were followed for 5 min and the movie loops 6 times. Note that the filopodia in the $foscrb_{Y10A}$ embryo move randomly and some filopodia, like the one label with the arrow (bottom embryo), appear to detach and move out of the plane. Time-lapse: 10 sec; 8 fps.

Video 4. Lateral views during germ band (GB) retraction in *w;foscrb,DE-cad::mTomato;*crb^{GX24} (top) and *w;*$foscrb_{Y10A}$*,DE-cad::mTomato;*crb^{GX24} (bottom) embryos. Time-lapse: 10 min; 8 fps.

Video 5. Dorsal views during GB retraction and the beginning of DC in *w;foscrb,DE-cad::GFP;*crb^{GX24} (top) and *w;*$foscrb_{Y10A}$*,DE-cad::GFP;*crb^{GX24} (bottom) embryos. Note that the yolk aggregates are clearly visible because they have an intense autofluorescence in the green part of the spectrum. Time-lapse: 10 min; 8 fps.

Video 6. Dorsal views during DC in *w;foscrb,*$GAL4^{332.3}$*/foscrb,UAS-Apoliner;*crb^{GX24} (first row), and two examples of *w;*$foscrb_{Y10A}$*,*$GAL4^{332.3}$*/*$foscrb_{Y10A}$*,UAS-Apoliner;*crb^{GX24} (second and third rows) embryos. Apoliner GFP signal is on the left (green), the RFP signal on the middle (magenta), and the merge on the right. At the time 210 min, the blinking arrows in the merge of the *foscrb* embryo indicate some apoptotic AS cells separated clearly. Time-lapse: 10 min; 8 fps.

Video 7. DC in $yrt^{\Delta 75a}$ zygotic mutants expressing the different fosmids. *w;foscrb,DE-cad::GFP;*$yrt^{\Delta 75a}crb^{11A22}$ (top) and *w;*$foscrb_{Y10A}$*,DE-cad::GFP;*$yrt^{\Delta 75a}crb^{11A22}$ (bottom) embryos. The arrow in the top embryo marks the characteristic defects in the posterior canthus observed during DC in $yrt^{\Delta 75a}$ zygotic mutants. In the *w;*$foscrb_{Y10A}$*,DE-cad::GFP;*$yrt^{\Delta 75a}crb^{11A22}$ embryo the GB retraction and the DC phenotypes are comparable to the ones in the *w;*$foscrb_{Y10A}$*,DE-cad::GFP;*crb^{GX24} (Video 2). Time-lapse: 6 min; 12 fps.

Video 8. Dorsal views during the pulsed contractions of AS cells in *w;foscrb,DE-cad::GFP;*crb^{GX24} (left) and *w;*$foscrb_{Y10A}$*,DE-cad::GFP;*crb^{GX24} (right). Time-lapse: 10 sec; 15 fps.

Video 9. Dorsal views during the pulsed contractions of AS cells in *w;foscrb/Zip::GFP;*crb^{GX24} (left) and *w;*$foscrb_{Y10A}$*/Zip::GFP;*crb^{GX24} (right). Time-lapse: 10 sec; 15 fps.

Video 10. Magnifications of a small group of cells shown in the Video 11 to see in more detail the medial foci accumulation of Zip::GFP during the cell contraction. These magnifications (2X from original) were created using a bicubic algorithm in Fiji. *w;foscrb/Zip::GFP;*crb^{GX24} (left) and *w;*$foscrb_{Y10A}$*/Zip::GFP;*crb^{GX24} (right). Time-lapse: 10 sec; 15 fps.

Video 11. Dorsal views during DC in embryos expressing the phosphatase Flw in the AS cells under the control of the $GAL4^{332.3}$ driver. The signal from the *UAS-Actin::RFP* is not shown. *w;foscrb,*$GAL4^{332.3}$*/UAS-flw-HA,DE-cad::GFP;*crb^{GX24}/crb^{11A22}*,UAS-Act::RFP* (top) and *w;*$foscrb_{Y10A}$*,*$GAL4^{332.3}$*/UAS-flw-HA,DE-cad::GFP;*crb^{GX24}/crb^{11A22}*,UAS-Act::RFP* (bottom). Time-lapse: 5 min; 12 fps.

Video 12. Flw expression in the AS of $foscrb_{Y10A}$ embryos suppresses the disruption of the ZA. Dorsal views during the pulsed contractions of AS cells. The signal from the *UAS-Actin::RFP* is not shown. (**A,B**) Embryos that do not express the Flw and are trans-heterozygous for *D*E-cad::GFP; (A) *w;foscrb/UAS-flw-HA,DE-cad::GFP;*crb^{GX24}/crb^{11A22}*,UAS-Act::RFP* and (B) *w;*$foscrb_{Y10A}$*/UAS-flw-HA,DE-cad::GFP;*crb^{GX24}/crb^{11A22}*,UAS-Act::RFP*. (**C,D**) Embryos that express Flw in the AS cells under the control of the $GAL4^{332.3}$ driver; (C) *w;foscrb,*$GAL4^{332.3}$*/UAS-flw-HA,DE-cad::GFP;*crb^{GX24}/crb^{11A22}*,UAS-Act::RFP* and (D) *w;*$foscrb_{Y10A}$*,*$GAL4^{332.3}$*/UAS-flw-HA,DE-cad::GFP;*crb^{GX24}/crb^{11A22}*,UAS-Act::RFP*. Time-lapse: 10 sec; 15 fps.

Video 13. Dorsal views during DC in embryos heterozygous for the $SCAR^{\Delta 37}$ allele. *w;foscrb,DE-cad::GFP/*$SCAR^{\Delta 37}$*,DE-cad::GFP;*crb^{GX24} (top) and *w;*$foscrb_{Y10A}$*,DE-cad::GFP/*$SCAR^{\Delta 37}$*,DE-cad::GFP;*crb^{GX24} (bottom). Time-lapse: 10 min; 8 fps.

Video 14. Dorsal views during DC in embryos heterozygous for the $Arp3^{EP3640}$ allele. *w;foscrb,DE-cad::GFP/+;*crb^{11A22}*,*$Arp3^{EP3640}/crb^{GX24}$ (top) and *w;*$foscrb_{Y10A}$*,DE-cad::GFP/+;*crb^{11A22}*,*$Arp3^{EP3640}/crb^{GX24}$ (bottom). Time-lapse: 10 min; 8 fps.

References.

Abreu-Blanco, M.T., J.M. Verboon, and S.M. Parkhurst. 2014. Coordination of Rho family GTPase activities to orchestrate cytoskeleton responses during cell wound repair. *Curr Biol*. 24:144–155. doi:10.1016/j.cub.2013.11.048.

Abreu-Blanco, M.T., J.M. Verboon, R. Liu, J.J. Watts, and S.M. Parkhurst. 2012. Drosophila embryos close epithelial wounds using a combination of cellular protrusions and an actomyosin purse string. *J Cell Sci*. 125:5984–5997. doi:10.1242/jcs.109066.

Afshar, K., B. Stuart, and S.A. Wasserman. 2000. Functional analysis of the Drosophila diaphanous FH protein in early embryonic development. *Development*. 127:1887–1897.

Akhtar, N., and N.A. Hotchin. 2001. RAC1 regulates adherens junctions through endocytosis of E-cadherin. *Mol Biol Cell*. 12:847–862.

Azevedo, D., M. Antunes, S. Prag, X. Ma, U. Hacker, G.W. Brodland, M.S. Hutson, J. Solon, and A. Jacinto. 2011. DRhoGEF2 Regulates Cellular Tension and Cell Pulsations in the Amnioserosa during Drosophila Dorsal Closure. *PLoS ONE*. 6:e23964. doi:10.1371/journal.pone.0023964.

Bachmann, A., M. Schneider, E. Theilenberg, F. Grawe, and E. Knust. 2001. Drosophila Stardust is a partner of Crumbs in the control of epithelial cell polarity. *Nature*. 414:638–643. doi:10.1038/414638a.

Bardet, P.-L., G. Kolahgar, A. Mynett, I. Miguel-Aliaga, J. Briscoe, P. Meier, and J.-P. Vincent. 2008. A fluorescent reporter of caspase activity for live imaging. *Proc Natl Acad Sci USA*. 105:13901–13905. doi:10.1073/pnas.0806983105.

Bazellières, E., E. Assémat, J.-P. Arsanto, A. Le Bivic, and D. Massey-Harroche. 2009. Crumbs proteins in epithelial morphogenesis. *Front Biosci*. 14:2149–2169.

Bertet, C., L. Sulak, and T. Lecuit. 2004. Myosin-dependent junction remodelling controls planar cell intercalation and axis elongation. *Nature*. 429:667–671. doi:10.1038/nature02590.

Bilancia, C.G., J.D. Winkelman, D. Tsygankov, S.H. Nowotarski, J.A. Sees, K. Comber, I. Evans, V. Lakhani, W. Wood, T.C. Elston, D.R. Kovar, and M. Peifer. 2014. Enabled negatively regulates diaphanous-driven actin dynamics in vitro and in vivo. *Dev Cell*. 28:394–408. doi:10.1016/j.devcel.2014.01.015.

Blanchard, G.B., S. Murugesu, R.J. Adams, A. Martinez-Arias, and N. Gorfinkiel. 2010. Cytoskeletal dynamics and supracellular organisation of cell shape fluctuations during dorsal closure. *Development*. 137:2743–2752. doi:10.1242/dev.045872.

Blanchoin, L., R. Boujemaa-Paterski, C. Sykes, and J. Plastino. 2014. Actin dynamics, architecture, and mechanics in cell motility. *Physiol Rev*. 94:235–263. doi:10.1152/physrev.00018.2013.

Boedigheimer, M., and A. Laughon. 1993. Expanded: a gene involved in the control of cell proliferation in imaginal discs. *Development*. 118:1291–1301.

Boettner, B., P. Harjes, S. Ishimaru, M. Heke, H.Q. Fan, Y. Qin, L. Van Aelst, and U. Gaul. 2003. The AF-6 homolog canoe acts as a Rap1 effector during dorsal closure of the Drosophila embryo. *Genetics*. 165:159–169.

Boggiano, J.C., and R.G. Fehon. 2012. Growth control by committee: intercellular junctions, cell polarity, and the cytoskeleton regulate hippo signaling. *Dev Cell*. 22:695–702. doi:10.1016/j.devcel.2012.03.013.

Braga, V.M., M. Betson, X. Li, and N. Lamarche-Vane. 2000. Activation of the small GTPase Rac is sufficient to disrupt cadherin-dependent cell-cell adhesion in normal human keratinocytes. *Mol Biol Cell*. 11:3703–3721.

Bulgakova, N.A., and E. Knust. 2009. The Crumbs complex: from epithelial-cell polarity to retinal degeneration. *J Cell Sci*. 122:2587–2596. doi:10.1242/jcs.023648.

Bulgakova, N.A., O. Kempkens, and E. Knust. 2008. Multiple domains of Stardust differentially mediate localisation of the Crumbs-Stardust complex during photoreceptor development in Drosophila. *J Cell Sci*. 121:2018–2026. doi:10.1242/jcs.031088.

1034 Buszczak, M., S. Paterno, D. Lighthouse, J. Bachman, J. Planck, S. Owen, A.D. Skora, T.G. Nystul, B. Ohlstein,
1035 A. Allen, J.E. Wilhelm, T.D. Murphy, R.W. Levis, E. Matunis, N. Srivali, R.A. Hoskins, and A.C.
1036 Spradling. 2007. The carnegie protein trap library: a versatile tool for Drosophila developmental studies.
1037 *Genetics*. 175:1505–1531. doi:10.1534/genetics.106.065961.

1038 Campos-Ortega, J.A., and V. Hartenstein. 1985. The Embryonic Development of *Drosophila melanogaster*.
1039 Springer-Verlag Berlin Heidelberg. 237 pp.

1040 Cheng, L., K. Itoh, and V. Lemmon. 2005. L1-mediated branching is regulated by two ezrin-radixin-moesin
1041 (ERM)-binding sites, the RSLE region and a novel juxtamembrane ERM-binding region. *J Neurosci*.
1042 25:395–403. doi:10.1523/JNEUROSCI.4097-04.2005.

1043 Choi, W., K.-C. Jung, K.S. Nelson, M.A. Bhat, G.J. Beitel, M. Peifer, and A.S. Fanning. 2011. The single
1044 Drosophila ZO-1 protein Polychaetoid regulates embryonic morphogenesis in coordination with
1045 Canoe/afadin and Enabled. *Mol Biol Cell*. 22:2010–2030. doi:10.1091/mbc.E10-12-1014.

1046 Conder, R., H. Yu, M. Ricos, H. Hing, W. Chia, L. Lim, and N. Harden. 2004. dPak is required for integrity of
1047 the leading edge cytoskeleton during Drosophila dorsal closure but does not signal through the JNK cascade.
1048 *Dev Biol*. 276:378–390. doi:10.1016/j.ydbio.2004.08.044.

1049 Conti, M.A., S. Even-Ram, C. Liu, K.M. Yamada, and R.S. Adelstein. 2004. Defects in cell adhesion and the
1050 visceral endoderm following ablation of nonmuscle myosin heavy chain II-A in mice. *J Biol Chem*.
1051 279:41263–41266. doi:10.1074/jbc.C400352200.

1052 David, D.J.V., A. Tishkina, and T.J.C. Harris. 2010. The PAR complex regulates pulsed actomyosin contractions
1053 during amnioserosa apical constriction in Drosophila. *Development*. 137:1645–1655.
1054 doi:10.1242/dev.044107.

1055 David, D.J.V., Q. Wang, J.J. Feng, and T.J.C. Harris. 2013. Bazooka inhibits aPKC to limit antagonism of
1056 actomyosin networks during amnioserosa apical constriction. *Development*. 140:4719–4729.
1057 doi:10.1242/dev.098491.

1058 Denholm, B., S. Brown, R.P. Ray, M. Ruiz-Gómez, H. Skaer, and J.C.-G. Hombría. 2005. crossveinless-c is a
1059 RhoGAP required for actin reorganisation during morphogenesis. *Development*. 132:2389–2400.
1060 doi:10.1242/dev.01829.

1061 Djiane, A., H. Shimizu, M. Wilkin, S. Mazleyrat, M.D. Jennings, J. Avis, S. Bray, and M. Baron. 2011. Su(dx)
1062 E3 ubiquitin ligase-dependent and -independent functions of polychaetoid, the Drosophila ZO-1 homologue.
1063 *J Cell Biol*. 192:189–200. doi:10.1083/jcb.201007023.

1064 Edwards, K.A., M. Demsky, R.A. Montague, N. Weymouth, and D.P. Kiehart. 1997. GFP-moesin illuminates
1065 actin cytoskeleton dynamics in living tissue and demonstrates cell shape changes during morphogenesis in
1066 Drosophila. *Dev Biol*. 191:103–117. doi:10.1006/dbio.1997.8707.

1067 Eltsov, M., N. Dubé, Z. Yu, L. Pasakarnis, U. Haselmann-Weiss, D. Brunner, and A.S. Frangakis. 2015.
1068 Quantitative analysis of cytoskeletal reorganization during epithelial tissue sealing by large-volume electron
1069 tomography. *Nat Cell Biol*. 17:605–614. doi:10.1038/ncb3159.

1070 Engl, W., B. Arasi, L.L. Yap, J.P. Thiery, and V. Viasnoff. 2014. Actin dynamics modulate mechanosensitive
1071 immobilization of E-cadherin at adherens junctions. *Nat Cell Biol*. 16:587–594. doi:10.1038/ncb2973.

1072 Firmino, J., J.-Y. Tinevez, and E. Knust. 2013. Crumbs affects protein dynamics in anterior regions of the
1073 developing Drosophila embryo. *PLoS ONE*. 8:e58839. doi:10.1371/journal.pone.0058839.

1074 Fischer, S.C., G.B. Blanchard, J. Duque, R.J. Adams, A.M. Arias, S.D. Guest, and N. Gorfinkiel. 2014.
1075 Contractile and mechanical properties of epithelia with perturbed actomyosin dynamics. *PLoS ONE*.
1076 9:e95695. doi:10.1371/journal.pone.0095695.

1077 Frank, L.H., and C. Rushlow. 1996. A group of genes required for maintenance of the amnioserosa tissue in
1078 Drosophila. *Development*. 122:1343–1352.

1079 Franke, J.D., R.A. Montague, and D.P. Kiehart. 2005. Nonmuscle myosin II generates forces that transmit
1080 tension and drive contraction in multiple tissues during dorsal closure. *Curr Biol*. 15:2208–2221.
1081 doi:10.1016/j.cub.2005.11.064.

Gates, J., J.P. Mahaffey, S.L. Rogers, M. Emerson, E.M. Rogers, S.L. Sottile, D. Van Vactor, F.B. Gertler, and M. Peifer. 2007. Enabled plays key roles in embryonic epithelial morphogenesis in Drosophila. *Development*. 134:2027–2039. doi:10.1242/dev.02849.

Genevet, A., and N. Tapon. 2011. The Hippo pathway and apico-basal cell polarity. *Biochem J*. 436:213–224. doi:10.1042/BJ20110217.

Georgiou, M., and B. Baum. 2010. Polarity proteins and Rho GTPases cooperate to spatially organise epithelial actin-based protrusions. *J Cell Sci*. 123:1089–1098. doi:10.1242/jcs.060772.

Georgiou, M., E. Marinari, J. Burden, and B. Baum. 2008. Cdc42, Par6, and aPKC regulate Arp2/3-mediated endocytosis to control local adherens junction stability. *Curr Biol*. 18:1631–1638. doi:10.1016/j.cub.2008.09.029.

Glise, B., H. Bourbon, and S. Noselli. 1995. hemipterous encodes a novel Drosophila MAP kinase kinase, required for epithelial cell sheet movement. *Cell*. 83:451–461.

Gorfinkiel, N., and A.M. Arias. 2007. Requirements for adherens junction components in the interaction between epithelial tissues during dorsal closure in Drosophila. *J Cell Sci*. 120:3289–3298. doi:10.1242/jcs.010850.

Gorfinkiel, N., G.B. Blanchard, R.J. Adams, and A. Martinez-Arias. 2009. Mechanical control of global cell behaviour during dorsal closure in Drosophila. *Development*. 136:1889–1898. doi:10.1242/dev.030866.

Gorfinkiel, N., S. Schamberg, and G.B. Blanchard. 2011. Integrative approaches to morphogenesis: lessons from dorsal closure. *Genesis*. 49:522–533. doi:10.1002/dvg.20704.

Grawe, F., A. Wodarz, B. Lee, E. Knust, and H. Skaer. 1996. The Drosophila genes crumbs and stardust are involved in the biogenesis of adherens junctions. *Development*. 122:951–959.

Hamada, K., T. Shimizu, S. Yonemura, S. Tsukita, S. Tsukita, and T. Hakoshima. 2003. Structural basis of adhesion-molecule recognition by ERM proteins revealed by the crystal structure of the radixin-ICAM-2 complex. *EMBO J*. 22:502–514. doi:10.1093/emboj/cdg039.

Harden, N., J. Lee, H.Y. Loh, Y.M. Ong, I. Tan, T. Leung, E. Manser, and L. Lim. 1996. A Drosophila homolog of the Rac- and Cdc42-activated serine/threonine kinase PAK is a potential focal adhesion and focal complex protein that colocalizes with dynamic actin structures. *Mol Cell Biol*. 16:1896–1908.

Harden, N., M. Ricos, K. Yee, J. Sanny, C. Langmann, H. Yu, W. Chia, and L. Lim. 2002. Drac1 and Crumbs participate in amnioserosa morphogenesis during dorsal closure in Drosophila. *J Cell Sci*. 115:2119–2129.

Harden, N., M. Ricos, Y.M. Ong, W. Chia, and L. Lim. 1999. Participation of small GTPases in dorsal closure of the Drosophila embryo: distinct roles for Rho subfamily proteins in epithelial morphogenesis. *J Cell Sci*. 112 (Pt 3):273–284.

Harris, T.J.C. 2012. Adherens junction assembly and function in the Drosophila embryo. *Int Rev Cell Mol Biol*. 293:45–83. doi:10.1016/B978-0-12-394304-0.00007-5.

Harris, T.J.C., and M. Peifer. 2005. The positioning and segregation of apical cues during epithelial polarity establishment in Drosophila. *J Cell Biol*. 170:813–823. doi:10.1083/jcb.200505127.

Heisenberg, C.-P., and Y. Bellaiche. 2013. Forces in tissue morphogenesis and patterning. *Cell*. 153:948–962. doi:10.1016/j.cell.2013.05.008.

Hipfner, D.R., N. Keller, and S.M. Cohen. 2004. Slik Sterile-20 kinase regulates Moesin activity to promote epithelial integrity during tissue growth. *Genes Dev*. 18:2243–2248. doi:10.1101/gad.303304.

Hofmann, C., M. Shepelev, and J. Chernoff. 2004. The genetics of Pak. *J Cell Sci*. 117:4343–4354. doi:10.1242/jcs.01392.

Homem, C.C.F., and M. Peifer. 2008. Diaphanous regulates myosin and adherens junctions to control cell contractility and protrusive behavior during morphogenesis. *Development*. 135:1005–1018. doi:10.1242/dev.016337.

1127 Homem, C.C.F., and M. Peifer. 2009. Exploring the roles of diaphanous and enabled activity in shaping the
1128 balance between filopodia and lamellipodia. *Mol Biol Cell*. 20:5138–5155. doi:10.1091/mbc.E09-02-0144.

1129 Hong, Y., B. Stronach, N. Perrimon, L.Y. Jan, and Y.N. Jan. 2001. Drosophila Stardust interacts with Crumbs to
1130 control polarity of epithelia but not neuroblasts. *Nature*. 414:634–638. doi:10.1038/414634a.

1131 Hoover, K.B., and P.J. Bryant. 2002. Drosophila Yurt is a new protein-4.1-like protein required for epithelial
1132 morphogenesis. *Dev Genes Evol*. 212:230–238. doi:10.1007/s00427-002-0231-6.

1133 Hou, X.S., E.S. Goldstein, and N. Perrimon. 1997. Drosophila Jun relays the Jun amino-terminal kinase signal
1134 transduction pathway to the Decapentaplegic signal transduction pathway in regulating epithelial cell sheet
1135 movement. *Genes Dev*. 11:1728–1737.

1136 Huang, J., L. Huang, Y.-J. Chen, E. Austin, C.E. Devor, F. Roegiers, and Y. Hong. 2011. Differential regulation
1137 of adherens junction dynamics during apical-basal polarization. *J Cell Sci*. 124:4001–4013.
1138 doi:10.1242/jcs.086694.

1139 Huang, J., W. Zhou, W. Dong, A.M. Watson, and Y. Hong. 2009. Directed, efficient, and versatile modifications
1140 of the Drosophila genome by genomic engineering. *Proc Natl Acad Sci USA*. 106:8284–8289.
1141 doi:10.1073/pnas.0900641106.

1142 Hudson, A.M., and L. Cooley. 2002. A subset of dynamic actin rearrangements in Drosophila requires the
1143 Arp2/3 complex. *J Cell Biol*. 156:677–687. doi:10.1083/jcb.200109065.

1144 Hutson, M.S., Y. Tokutake, M.-S. Chang, J.W. Bloor, S. Venakides, D.P. Kiehart, and G.S. Edwards. 2003.
1145 Forces for morphogenesis investigated with laser microsurgery and quantitative modeling. *Science*.
1146 300:145–149. doi:10.1126/science.1079552.

1147 Ivanova, M.E., G.C. Fletcher, N. O'Reilly, A.G. Purkiss, B.J. Thompson, and N.Q. McDonald. 2015. Structures
1148 of the human Pals1 PDZ domain with and without ligand suggest gated access of Crb to the PDZ peptide-
1149 binding groove. *Acta Crystallogr. D Biol. Crystallogr.* 71:555–564. doi:10.1107/S139900471402776X.

1150 Jacinto, A., W. Wood, S. Woolner, C. Hiley, L. Turner, C. Wilson, A. Martinez-Arias, and P. Martin. 2002.
1151 Dynamic analysis of actin cable function during Drosophila dorsal closure. *Curr Biol*. 12:1245–1250.

1152 Jacinto, A., W. Wood, T. Balayo, M. Turmaine, A. Martinez-Arias, and P. Martin. 2000. Dynamic actin-based
1153 epithelial adhesion and cell matching during Drosophila dorsal closure. *Curr Biol*. 10:1420–1426.

1154 Jayasinghe, A.K., S.M. Crews, D.N. Mashburn, and M.S. Hutson. 2013. Apical oscillations in amnioserosa cells:
1155 basolateral coupling and mechanical autonomy. *Biophys J*. 105:255–265. doi:10.1016/j.bpj.2013.05.027.

1156 Jürgens, G., E. Wieschaus, C. Nüsslein-Volhard, and H. Kluding. 1984. Mutations affecting the pattern of the
1157 larval cuticle in Drosophila melanogaster. *Dev Genes Evol*. 193:283–295.

1158 Kaltschmidt, J.A., N. Lawrence, V. Morel, T. Balayo, B.G. Fernández, A. Pelissier, A. Jacinto, and A. Martinez-
1159 Arias. 2002. Planar polarity and actin dynamics in the epidermis of Drosophila. *Nat Cell Biol*. 4:937–944.
1160 doi:10.1038/ncb882.

1161 Kempkens, O., E. Médina, G. Fernandez-Ballester, S. Ozüyaman, A. Le Bivic, L. Serrano, and E. Knust. 2006.
1162 Computer modelling in combination with in vitro studies reveals similar binding affinities of Drosophila
1163 Crumbs for the PDZ domains of Stardust and DmPar-6. *Eur J Cell Biol*. 85:753–767.
1164 doi:10.1016/j.ejcb.2006.03.003.

1165 Kiehart, D.P., C.G. Galbraith, K.A. Edwards, W.L. Rickoll, and R.A. Montague. 2000. Multiple forces
1166 contribute to cell sheet morphogenesis for dorsal closure in Drosophila. *J Cell Biol*. 149:471–490.

1167 Klebes, A., and E. Knust. 2000. A conserved motif in Crumbs is required for E-cadherin localisation and zonula
1168 adherens formation in Drosophila. *Curr Biol*. 10:76–85.

1169 Klose, S., D. Flores-Benitez, F. Riedel, and E. Knust. 2013. Fosmid-based structure-function analysis reveals
1170 functionally distinct domains in the cytoplasmic domain of Drosophila crumbs. *G3 (Bethesda)*. 3:153–165.
1171 doi:10.1534/g3.112.005074.

1172 Kockel, L., J. Zeitlinger, L.M. Staszewski, M. Mlodzik, and D. Bohmann. 1997. Jun in Drosophila development:

redundant and nonredundant functions and regulation by two MAPK signal transduction pathways. *Genes Dev*. 11:1748–1758.

Kolahgar, G., P.-L. Bardet, P.F. Langton, C. Alexandre, and J.-P. Vincent. 2011. Apical deficiency triggers JNK-dependent apoptosis in the embryonic epidermis of Drosophila. *Development*. 138:3021–3031. doi:10.1242/dev.059980.

Kovacs, E.M., M. Goodwin, R.G. Ali, A.D. Paterson, and A.S. Yap. 2002. Cadherin-directed actin assembly: E-cadherin physically associates with the Arp2/3 complex to direct actin assembly in nascent adhesive contacts. *Curr Biol*. 12:379–382.

Krajcovic, M.M., and J.S. Minden. 2012. Assessing the critical period for Rho kinase activity during Drosophila ventral furrow formation. *Dev Dyn*. 241:1729–1743. doi:10.1002/dvdy.23859.

Kurisu, S., and T. Takenawa. 2009. The WASP and WAVE family proteins. *Genome Biol*. 10:226. doi:10.1186/gb-2009-10-6-226.

Lamka, M.L., and H.D. Lipshitz. 1999. Role of the amnioserosa in germ band retraction of the Drosophila melanogaster embryo. *Dev Biol*. 214:102–112. doi:10.1006/dbio.1999.9409.

Laplante, C., and L.A. Nilson. 2006. Differential expression of the adhesion molecule Echinoid drives epithelial morphogenesis in Drosophila. *Development*. 133:3255–3264. doi:10.1242/dev.02492.

Laplante, C., and L.A. Nilson. 2011. Asymmetric distribution of Echinoid defines the epidermal leading edge during Drosophila dorsal closure. *J Cell Biol*. 192:335–348. doi:10.1083/jcb.201009022.

Laprise, P., S. Beronja, N.F. Silva-Gagliardi, M. Pellikka, A.M. Jensen, C.J. McGlade, and U. Tepass. 2006. The FERM protein Yurt is a negative regulatory component of the Crumbs complex that controls epithelial polarity and apical membrane size. *Dev Cell*. 11:363–374. doi:10.1016/j.devcel.2006.06.001.

Lecuit, T., and A.S. Yap. 2015. E-cadherin junctions as active mechanical integrators in tissue dynamics. *Nat Cell Biol*. 17:533–539. doi:10.1038/ncb3136.

Lecuit, T., P.-F. Lenne, and E. Munro. 2011. Force Generation, Transmission, and Integration during Cell and Tissue Morphogenesis. *Annu Rev Cell Dev Biol*. 27:157–184. doi:10.1146/annurev-cellbio-100109-104027.

Leibfried, A., R. Fricke, M.J. Morgan, S. Bogdan, and Y. Bellaiche. 2008. Drosophila Cip4 and WASp define a branch of the Cdc42-Par6-aPKC pathway regulating E-cadherin endocytosis. *Curr Biol*. 18:1639–1648. doi:10.1016/j.cub.2008.09.063.

Levayer, R., A. Pelissier-Monier, and T. Lecuit. 2011. Spatial regulation of Dia and Myosin-II by RhoGEF2 controls initiation of E-cadherin endocytosis during epithelial morphogenesis. *Nat Cell Biol*. 13:529–540. doi:10.1038/ncb2224.

Li, Y., Z. Wei, Y. Yan, Q. Wan, Q. Du, and M. Zhang. 2014. Structure of Crumbs tail in complex with the PALS1 PDZ-SH3-GK tandem reveals a highly specific assembly mechanism for the apical Crumbs complex. *Proc Natl Acad Sci USA*. 111:17444–17449. doi:10.1073/pnas.1416515111.

Lin, H.-P., H.-M. Chen, S.-Y. Wei, L.-Y. Chen, L.-H. Chang, Y.-J. Sun, S.-Y. Huang, and J.-C. Hsu. 2007. Cell adhesion molecule Echinoid associates with unconventional myosin VI/Jaguar motor to regulate cell morphology during dorsal closure in Drosophila. *Dev Biol*. 311:423–433. doi:10.1016/j.ydbio.2007.08.043.

Ling, C., Y. Zheng, F. Yin, J. Yu, J. Huang, Y. Hong, S. Wu, and D. Pan. 2010. The apical transmembrane protein Crumbs functions as a tumor suppressor that regulates Hippo signaling by binding to Expanded. *Proc Natl Acad Sci USA*. 107:10532–10537. doi:10.1073/pnas.1004279107.

Liu, K.C., and R.E. Cheney. 2012. Myosins in cell junctions. *Bioarchitecture*. 2:158–170. doi:10.4161/bioa.21791.

Liu, R., E.V. Linardopoulou, G.E. Osborn, and S.M. Parkhurst. 2010. Formins in development: orchestrating body plan origami. *Biochim Biophys Acta*. 1803:207–225. doi:10.1016/j.bbamcr.2008.09.016.

Loie, E., L.E. Charrier, K. Sollier, J.-Y. Masson, and P. Laprise. 2015. CRB3A Controls the Morphology and Cohesion of Cancer Cells through Ehm2/p114RhoGEF-Dependent Signaling. *Mol Cell Biol*. 35:3423–3435.

doi:10.1128/MCB.00673-15.

Lozano, E., M.A.M. Frasa, K. Smolarczyk, U.G. Knaus, and V.M.M. Braga. 2008. PAK is required for the disruption of E-cadherin adhesion by the small GTPase Rac. *J Cell Sci*. 121:933–938. doi:10.1242/jcs.016121.

Lynch, H.E., S.M. Crews, B. Rosenthal, E. Kim, R. Gish, K. Echiverri, and M.S. Hutson. 2013. Cellular mechanics of germ band retraction in Drosophila. *Dev Biol*. 384:205–213. doi:10.1016/j.ydbio.2013.10.005.

Madhavan, M.M., and K. Madhavan. 1980. Morphogenesis of the epidermis of adult abdomen of Drosophila. *Journal of Embryology and Experimental Morphology*. 60:1–31.

Magie, C.R., D. Pinto-Santini, and S.M. Parkhurst. 2002. Rho1 interacts with p120ctn and alpha-catenin, and regulates cadherin-based adherens junction components in Drosophila. *Development*. 129:3771–3782.

Magie, C.R., M.R. Meyer, M.S. Gorsuch, and S.M. Parkhurst. 1999. Mutations in the Rho1 small GTPase disrupt morphogenesis and segmentation during early Drosophila development. *Development*. 126:5353–5364.

Marcinkevicius, E., and J.A. Zallen. 2013. Regulation of cytoskeletal organization and junctional remodeling by the atypical cadherin Fat. *Development*. 140:433–443. doi:10.1242/dev.083949.

Martín-Blanco, E., A. Gampel, J. Ring, K. Virdee, N. Kirov, A.M. Tolkovsky, and A. Martinez Arias. 1998. puckered encodes a phosphatase that mediates a feedback loop regulating JNK activity during dorsal closure in Drosophila. *Genes Dev*. 12:557–570.

Mason, F.M., M. Tworoger, and A.C. Martin. 2013. Apical domain polarization localizes actin-myosin activity to drive ratchet-like apical constriction. *Nat Cell Biol*. 15:926–936. doi:10.1038/ncb2796.

Matsubayashi, Y., C. Coulson-Gilmer, and T.H. Millard. 2015. Endocytosis-dependent coordination of multiple actin regulators is required for wound healing. *J Cell Biol*. 210:419–433. doi:10.1083/jcb.201411037.

Matusek, T., A. Djiane, F. Jankovics, D. Brunner, M. Mlodzik, and J. Mihály. 2006. The Drosophila formin DAAM regulates the tracheal cuticle pattern through organizing the actin cytoskeleton. *Development*. 133:957–966. doi:10.1242/dev.02266.

McEwen, D.G., R.T. Cox, and M. Peifer. 2000. The canonical Wg and JNK signaling cascades collaborate to promote both dorsal closure and ventral patterning. *Development*. 127:3607–3617.

Menzel, N., D. Schneeberger, and T. Raabe. 2007. The Drosophila p21 activated kinase Mbt regulates the actin cytoskeleton and adherens junctions to control photoreceptor cell morphogenesis. *Mech Dev*. 124:78–90. doi:10.1016/j.mod.2006.09.007.

Menzel, N., J. Melzer, J. Waschke, C. Lenz, H. Wecklein, G. Lochnit, D. Drenckhahn, and T. Raabe. 2008. The Drosophila p21-activated kinase Mbt modulates DE-cadherin-mediated cell adhesion by phosphorylation of Armadillo. *Biochem J*. 416:231–241. doi:10.1042/BJ20080465.

Médina, E., J. Williams, E. Klipfell, D. Zarnescu, G. Thomas, and A. Le Bivic. 2002. Crumbs interacts with moesin and beta(Heavy)-spectrin in the apical membrane skeleton of Drosophila. *J Cell Biol*. 158:941–951. doi:10.1083/jcb.200203080.

Mizuno, T., M. Amano, K. Kaibuchi, and Y. Nishida. 1999. Identification and characterization of Drosophila homolog of Rho-kinase. *Gene*. 238:437–444.

Morais-de-Sá, E., V. Mirouse, and D. St Johnston. 2010. aPKC phosphorylation of Bazooka defines the apical/lateral border in Drosophila epithelial cells. *Cell*. 141:509–523. doi:10.1016/j.cell.2010.02.040.

Morin, X., R. Daneman, M. Zavortink, and W. Chia. 2001. A protein trap strategy to detect GFP-tagged proteins expressed from their endogenous loci in Drosophila. *Proc Natl Acad Sci USA*. 98:15050–15055. doi:10.1073/pnas.261408198.

Muliyil, S., P. Krishnakumar, and M. Narasimha. 2011. Spatial, temporal and molecular hierarchies in the link between death, delamination and dorsal closure. *Development*. 138:3043–3054. doi:10.1242/dev.060731.

Muschalik, N., and E. Knust. 2011. Increased levels of the cytoplasmic domain of Crumbs repolarise developing Drosophila photoreceptors. *J Cell Sci*. 124:3715–3725. doi:10.1242/jcs.091223.

Neisch, A.L., O. Speck, B. Stronach, and R.G. Fehon. 2010. Rho1 regulates apoptosis via activation of the JNK signaling pathway at the plasma membrane. *J Cell Biol*. 189:311–323. doi:10.1083/jcb.200912010.

Ninov, N., D.A. Chiarelli, and E. Martín-Blanco. 2007. Extrinsic and intrinsic mechanisms directing epithelial cell sheet replacement during Drosophila metamorphosis. *Development*. 134:367–379. doi:10.1242/dev.02728.

Nowotarski, S.H., N. McKeon, R.J. Moser, and M. Peifer. 2014. The actin regulators Enabled and Diaphanous direct distinct protrusive behaviors in different tissues during Drosophila development. *Mol Biol Cell*. 25:3147–3165. doi:10.1091/mbc.E14-05-0951.

Paluch, E., and C.-P. Heisenberg. 2009. Biology and physics of cell shape changes in development. *Curr Biol*. 19:R790–9. doi:10.1016/j.cub.2009.07.029.

Pellikka, M., G. Tanentzapf, M. Pinto, C. Smith, C.J. McGlade, D.F. Ready, and U. Tepass. 2002. Crumbs, the Drosophila homologue of human CRB1/RP12, is essential for photoreceptor morphogenesis. *Nature*. 416:143–149. doi:10.1038/nature721.

Pickering, K., J. Alves-Silva, D. Goberdhan, and T.H. Millard. 2013. Par3/Bazooka and phosphoinositides regulate actin protrusion formation during Drosophila dorsal closure and wound healing. *Development*. 140:800–809. doi:10.1242/dev.089557.

Pirraglia, C., J. Walters, and M.M. Myat. 2010. Pak1 control of E-cadherin endocytosis regulates salivary gland lumen size and shape. *Development*. 137:4177–4189. doi:10.1242/dev.048827.

Pokutta, S., F. Drees, Y. Takai, W.J. Nelson, and W.I. Weis. 2002. Biochemical and structural definition of the l-afadin- and actin-binding sites of alpha-catenin. *J Biol Chem*. 277:18868–18874. doi:10.1074/jbc.M201463200.

Quiros, M., and A. Nusrat. 2014. RhoGTPases, actomyosin signaling and regulation of the Epithelial Apical Junctional Complex. *Semin Cell Dev Biol*. 36C:194–203. doi:10.1016/j.semcdb.2014.09.003.

Raghavan, S., I. Williams, H. Aslam, D. Thomas, B. Szöor, G. Morgan, S. Gross, J. Turner, J. Fernandes, K. VijayRaghavan, and L. Alphey. 2000. Protein phosphatase 1β is required for the maintenance of muscle attachments. *Current Biology*. 10:269–272. doi:10.1016/S0960-9822(00)00364-X.

Rauzi, M., P.-F. Lenne, and T. Lecuit. 2010. Planar polarized actomyosin contractile flows control epithelial junction remodelling. *Nature*. 468:1110–1114. doi:10.1038/nature09566.

Reed, B.H., R. Wilk, and H.D. Lipshitz. 2001. Downregulation of Jun kinase signaling in the amnioserosa is essential for dorsal closure of the Drosophila embryo. *Curr Biol*. 11:1098–1108.

Reed, B.H., R. Wilk, F. Schöck, and H.D. Lipshitz. 2004. Integrin-dependent apposition of Drosophila extraembryonic membranes promotes morphogenesis and prevents anoikis. *Curr Biol*. 14:372–380. doi:10.1016/j.cub.2004.02.029.

Richard, M., F. Grawe, and E. Knust. 2006. DPATJ plays a role in retinal morphogenesis and protects against light-dependent degeneration of photoreceptor cells in the Drosophila eye. *Dev Dyn*. 235:895–907. doi:10.1002/dvdy.20595.

Richard, M., N. Muschalik, F. Grawe, S. Ozüyaman, and E. Knust. 2009. A role for the extracellular domain of Crumbs in morphogenesis of Drosophila photoreceptor cells. *Eur J Cell Biol*. 88:765–777. doi:10.1016/j.ejcb.2009.07.006.

Ricos, M.G., N. Harden, K.P. Sem, L. Lim, and W. Chia. 1999. Dcdc42 acts in TGF-beta signaling during Drosophila morphogenesis: distinct roles for the Drac1/JNK and Dcdc42/TGF-beta cascades in cytoskeletal regulation. *J Cell Sci*. 112 (Pt 8):1225–1235.

Riesgo-Escovar, J.R., M. Jenni, A. Fritz, and E. Hafen. 1996. The Drosophila Jun-N-terminal kinase is required for cell morphogenesis but not for DJun-dependent cell fate specification in the eye. *Genes Dev*. 10:2759–2768.

Ring, J.M., and A. Martinez Arias. 1993. puckered, a gene involved in position-specific cell differentiation in the dorsal epidermis of the Drosophila larva. *Dev Suppl*. 251–259.

Ríos-Barrera, L.D., and J.R. Riesgo-Escovar. 2013. Regulating cell morphogenesis: the Drosophila Jun N-terminal kinase pathway. *Genesis*. 51:147–162. doi:10.1002/dvg.22354.

Robinson, B.S., J. Huang, Y. Hong, and K.H. Moberg. 2010. Crumbs regulates Salvador/Warts/Hippo signaling in Drosophila via the FERM-domain protein Expanded. *Curr Biol*. 20:582–590. doi:10.1016/j.cub.2010.03.019.

Rodriguez-Boulan, E., and I.G. Macara. 2014. Organization and execution of the epithelial polarity programme. *Nat Rev Mol Cell Biol*. 15:225–242. doi:10.1038/nrm3775.

Rodriguez-Diaz, A., Y. Toyama, D.L. Abravanel, J.M. Wiemann, A.R. Wells, U.S. Tulu, G.S. Edwards, and D.P. Kiehart. 2008. Actomyosin purse strings: renewable resources that make morphogenesis robust and resilient. *HFSP J*. 2:220–237. doi:10.2976/1.2955565.

Roh, M.H., O. Makarova, C.-J. Liu, K. Shin, S. Lee, S. Laurinec, M. Goyal, R. Wiggins, and B. Margolis. 2002. The Maguk protein, Pals1, functions as an adapter, linking mammalian homologues of Crumbs and Discs Lost. *J Cell Biol*. 157:161–172. doi:10.1083/jcb.200109010.

Roh-Johnson, M., G. Shemer, C.D. Higgins, J.H. McClellan, A.D. Werts, U.S. Tulu, L. Gao, E. Betzig, D.P. Kiehart, and B. Goldstein. 2012. Triggering a cell shape change by exploiting preexisting actomyosin contractions. *Science*. 335:1232–1235. doi:10.1126/science.1217869.

Rotty, J.D., C. Wu, and J.E. Bear. 2013. New insights into the regulation and cellular functions of the ARP2/3 complex. *Nat Rev Mol Cell Biol*. 14:7–12. doi:10.1038/nrm3492.

Saias, L., J. Swoger, A. D'Angelo, P. Hayes, J. Colombelli, J. Sharpe, G. Salbreux, and J. Solon. 2015. Decrease in Cell Volume Generates Contractile Forces Driving Dorsal Closure. *Dev Cell*. 33:611–621. doi:10.1016/j.devcel.2015.03.016.

Sarpal, R., M. Pellikka, R.R. Patel, F.Y.W. Hui, D. Godt, and U. Tepass. 2012. Mutational analysis supports a core role for Drosophila α-catenin in adherens junction function. *J Cell Sci*. 125:233–245. doi:10.1242/jcs.096644.

Sawyer, J.K., N.J. Harris, K.C. Slep, U. Gaul, and M. Peifer. 2009. The Drosophila afadin homologue Canoe regulates linkage of the actin cytoskeleton to adherens junctions during apical constriction. *J Cell Biol*. 186:57–73. doi:10.1083/jcb.200904001.

Sawyer, J.K., W. Choi, K.-C. Jung, L. He, N.J. Harris, and M. Peifer. 2011. A contractile actomyosin network linked to adherens junctions by Canoe/afadin helps drive convergent extension. *Mol Biol Cell*. 22:2491–2508. doi:10.1091/mbc.E11-05-0411.

Schindelin, J., I. Arganda-Carreras, E. Frise, V. Kaynig, M. Longair, T. Pietzsch, S. Preibisch, C. Rueden, S. Saalfeld, B. Schmid, J.-Y. Tinevez, D.J. White, V. Hartenstein, K. Eliceiri, P. Tomancak, and A. Cardona. 2012. Fiji: an open-source platform for biological-image analysis. *Nat Methods*. 9:676–682. doi:10.1038/nmeth.2019.

Scuderi, A., and A. Letsou. 2005. Amnioserosa is required for dorsal closure in Drosophila. *Dev Dyn*. 232:791–800. doi:10.1002/dvdy.20306.

Shen, W., X. Chen, O. Cormier, D.C.-P. Cheng, B. Reed, and N. Harden. 2013. Modulation of Morphogenesis by Egfr during Dorsal Closure in Drosophila. *PLoS ONE*. 8:e60180. doi:10.1371/journal.pone.0060180.

Sherrard, K.M., and R.G. Fehon. 2015. The transmembrane protein Crumbs displays complex dynamics during follicular morphogenesis and is regulated competitively by Moesin and aPKC. *Development*. 142:1869–1878. doi:10.1242/dev.115329.

Simões, S. de M., J.T. Blankenship, O. Weitz, D.L. Farrell, M. Tamada, R. Fernandez-Gonzalez, and J.A. Zallen. 2010. Rho-kinase directs Bazooka/Par-3 planar polarity during Drosophila axis elongation. *Dev Cell*. 19:377–388. doi:10.1016/j.devcel.2010.08.011.

Sokolow, A., Y. Toyama, D.P. Kiehart, and G.S. Edwards. 2012. Cell ingression and apical shape oscillations

during dorsal closure in Drosophila. *Biophys J*. 102:969–979. doi:10.1016/j.bpj.2012.01.027.

Solon, J., A. Kaya-Copur, J. Colombelli, and D. Brunner. 2009. Pulsed forces timed by a ratchet-like mechanism drive directed tissue movement during dorsal closure. *Cell*. 137:1331–1342. doi:10.1016/j.cell.2009.03.050.

Speck, O., S.C. Hughes, N.K. Noren, R.M. Kulikauskas, and R.G. Fehon. 2003. Moesin functions antagonistically to the Rho pathway to maintain epithelial integrity. *Nature*. 421:83–87. doi:10.1038/nature01295.

Stronach, B.E., and N. Perrimon. 2001. Investigation of leading edge formation at the interface of amnioserosa and dorsal ectoderm in the Drosophila embryo. *Development*. 128:2905–2913.

Szymaniak, A.D., J.E. Mahoney, W.V. Cardoso, and X. Varelas. 2015. Crumbs3-Mediated Polarity Directs Airway Epithelial Cell Fate through the Hippo Pathway Effector Yap. *Dev Cell*. 34:283–296. doi:10.1016/j.devcel.2015.06.020.

Takahashi, K., T. Matsuo, T. Katsube, R. Ueda, and D. Yamamoto. 1998. Direct binding between two PDZ domain proteins Canoe and ZO-1 and their roles in regulation of the jun N-terminal kinase pathway in Drosophila morphogenesis. *Mech Dev*. 78:97–111.

Tan, J.L., S. Ravid, and J.A. Spudich. 1992. Control of nonmuscle myosins by phosphorylation. *Annu Rev Biochem*. 61:721–759. doi:10.1146/annurev.bi.61.070192.003445.

Tepass, U. 1996. Crumbs, a component of the apical membrane, is required for zonula adherens formation in primary epithelia of Drosophila. *Dev Biol*. 177:217–225. doi:10.1006/dbio.1996.0157.

Tepass, U. 2012. The apical polarity protein network in Drosophila epithelial cells: regulation of polarity, junctions, morphogenesis, cell growth, and survival. *Annu Rev Cell Dev Biol*. 28:655–685. doi:10.1146/annurev-cellbio-092910-154033.

Tepass, U., and E. Knust. 1990. Phenotypic and developmental analysis of mutations at the crumbs locus, a gene required for the development of epithelia in Drosophila melanogaster. *Roux's Arch Dev Biol*. 199:189–206. doi:10.1007/BF01682078.

Tepass, U., and E. Knust. 1993. Crumbs and stardust act in a genetic pathway that controls the organization of epithelia in Drosophila melanogaster. *Dev Biol*. 159:311–326. doi:10.1006/dbio.1993.1243.

Tepass, U., C. Theres, and E. Knust. 1990. crumbs encodes an EGF-like protein expressed on apical membranes of Drosophila epithelial cells and required for organization of epithelia. *Cell*. 61:787–799.

Tepass, U., E. Gruszynski-DeFeo, T.A. Haag, L. Omatyar, T. Török, and V. Hartenstein. 1996. shotgun encodes Drosophila E-cadherin and is preferentially required during cell rearrangement in the neurectoderm and other morphogenetically active epithelia. *Genes Dev*. 10:672–685.

Toyama, Y., X.G. Peralta, A.R. Wells, D.P. Kiehart, and G.S. Edwards. 2008. Apoptotic force and tissue dynamics during Drosophila embryogenesis. *Science*. 321:1683–1686. doi:10.1126/science.1157052.

Truong Quang, B.-A., M. Mani, O. Markova, T. Lecuit, and P.-F. Lenne. 2013. Principles of E-cadherin supramolecular organization in vivo. *Curr Biol*. 23:2197–2207. doi:10.1016/j.cub.2013.09.015.

Veltman, D.M., and R.H. Insall. 2010. WASP family proteins: their evolution and its physiological implications. *Mol Biol Cell*. 21:2880–2893. doi:10.1091/mbc.E10-04-0372.

Vereshchagina, N., D. Bennett, B. Szöor, J. Kirchner, S. Gross, E. Vissi, H. White-Cooper, and L. Alphey. 2004. The essential role of PP1beta in Drosophila is to regulate nonmuscle myosin. *Mol Biol Cell*. 15:4395–4405. doi:10.1091/mbc.E04-02-0139.

Verma, S., S.P. Han, M. Michael, G.A. Gomez, Z. Yang, R.D. Teasdale, A. Ratheesh, E.M. Kovacs, R.G. Ali, and A.S. Yap. 2012. A WAVE2-Arp2/3 actin nucleator apparatus supports junctional tension at the epithelial zonula adherens. *Mol Biol Cell*. 23:4601–4610. doi:10.1091/mbc.E12-08-0574.

Vicente-Manzanares, M., X. Ma, R.S. Adelstein, and A.R. Horwitz. 2009. Non-muscle myosin II takes centre stage in cell adhesion and migration. *Nat Rev Mol Cell Biol*. 10:778–790. doi:10.1038/nrm2786.

1403 Warner, S.J., H. Yashiro, and G.D. Longmore. 2010. The Cdc42/Par6/aPKC polarity complex regulates
1404 apoptosis-induced compensatory proliferation in epithelia. *Curr Biol*. 20:677–686.
1405 doi:10.1016/j.cub.2010.03.025.

1406 Watanabe, T., K. Sato, and K. Kaibuchi. 2009. Cadherin-mediated intercellular adhesion and signaling cascades
1407 involving small GTPases. *Cold Spring Harb Perspect Biol*. 1:a003020. doi:10.1101/cshperspect.a003020.

1408 Wei, Z., Y. Li, F. Ye, and M. Zhang. 2015. Structural Basis for the Phosphorylation-regulated Interaction
1409 between the Cytoplasmic Tail of Cell Polarity Protein Crumbs and the Actin-binding Protein Moesin. *J Biol*
1410 *Chem*. 290:11384–11392. doi:10.1074/jbc.M115.643791.

1411 Wells, A.R., R.S. Zou, U.S. Tulu, A.C. Sokolow, J.M. Crawford, G.S. Edwards, and D.P. Kiehart. 2014.
1412 Complete canthi removal reveals that forces from the amnioserosa alone are sufficient to drive dorsal
1413 closure in Drosophila. *Mol Biol Cell*. 25:3552–3568. doi:10.1091/mbc.E14-07-1190.

1414 Whiteman, E.L., S. Fan, J.L. Harder, K.D. Walton, C.-J. Liu, A. Soofi, V.C. Fogg, M.B. Hershenson, G.R.
1415 Dressler, G.H. Deutsch, D.L. Gumucio, and B. Margolis. 2014. Crumbs3 is essential for proper epithelial
1416 development and viability. *Mol Cell Biol*. 34:43–56. doi:10.1128/MCB.00999-13.

1417 Winter, C.G., B. Wang, A. Ballew, A. Royou, R. Karess, J.D. Axelrod, and L. Luo. 2001. Drosophila Rho-
1418 associated kinase (Drok) links Frizzled-mediated planar cell polarity signaling to the actin cytoskeleton.
1419 *Cell*. 105:81–91.

1420 Wodarz, A., U. Hinz, M. Engelbert, and E. Knust. 1995. Expression of crumbs confers apical character on
1421 plasma membrane domains of ectodermal epithelia of Drosophila. *Cell*. 82:67–76.

1422 Wood, W., A. Jacinto, R. Grose, S. Woolner, J. Gale, C. Wilson, and P. Martin. 2002. Wound healing
1423 recapitulates morphogenesis in Drosophila embryos. *Nat Cell Biol*. 4:907–912. doi:10.1038/ncb875.

1424 Xiao, Z., J. Patrakka, M. Nukui, L. Chi, D. Niu, C. Betsholtz, T. Pikkarainan, S. Vainio, and K. Tryggvason.
1425 2011. Deficiency in crumbs homolog 2 (Crb2) affects gastrulation and results in embryonic lethality in
1426 mice. *Dev Dyn*. 240:2646–2656. doi:10.1002/dvdy.22778.

1427 Yashiro, H., A.J. Loza, J.B. Skeath, and G.D. Longmore. 2014. Rho1 regulates adherens junction remodeling by
1428 promoting recycling endosome formation through activation of myosin II. *Mol Biol Cell*. 25:2956–2969.
1429 doi:10.1091/mbc.E14-04-0894.

1430 Yip, M.L., M.L. Lamka, and H.D. Lipshitz. 1997. Control of germ-band retraction in Drosophila by the zinc-
1431 finger protein HINDSIGHT. *Development*. 124:2129–2141.

1432 Young, P.E., A.M. Richman, A.S. Ketchum, and D.P. Kiehart. 1993. Morphogenesis in Drosophila requires
1433 nonmuscle myosin heavy chain function. *Genes Dev*. 7:29–41.

1434 Zallen, J.A., Y. Cohen, A.M. Hudson, L. Cooley, E. Wieschaus, and E.D. Schejter. 2002. SCAR is a primary
1435 regulator of Arp2/3-dependent morphological events in Drosophila. *J Cell Biol*. 156:689–701.
1436 doi:10.1083/jcb.200109057.

1437

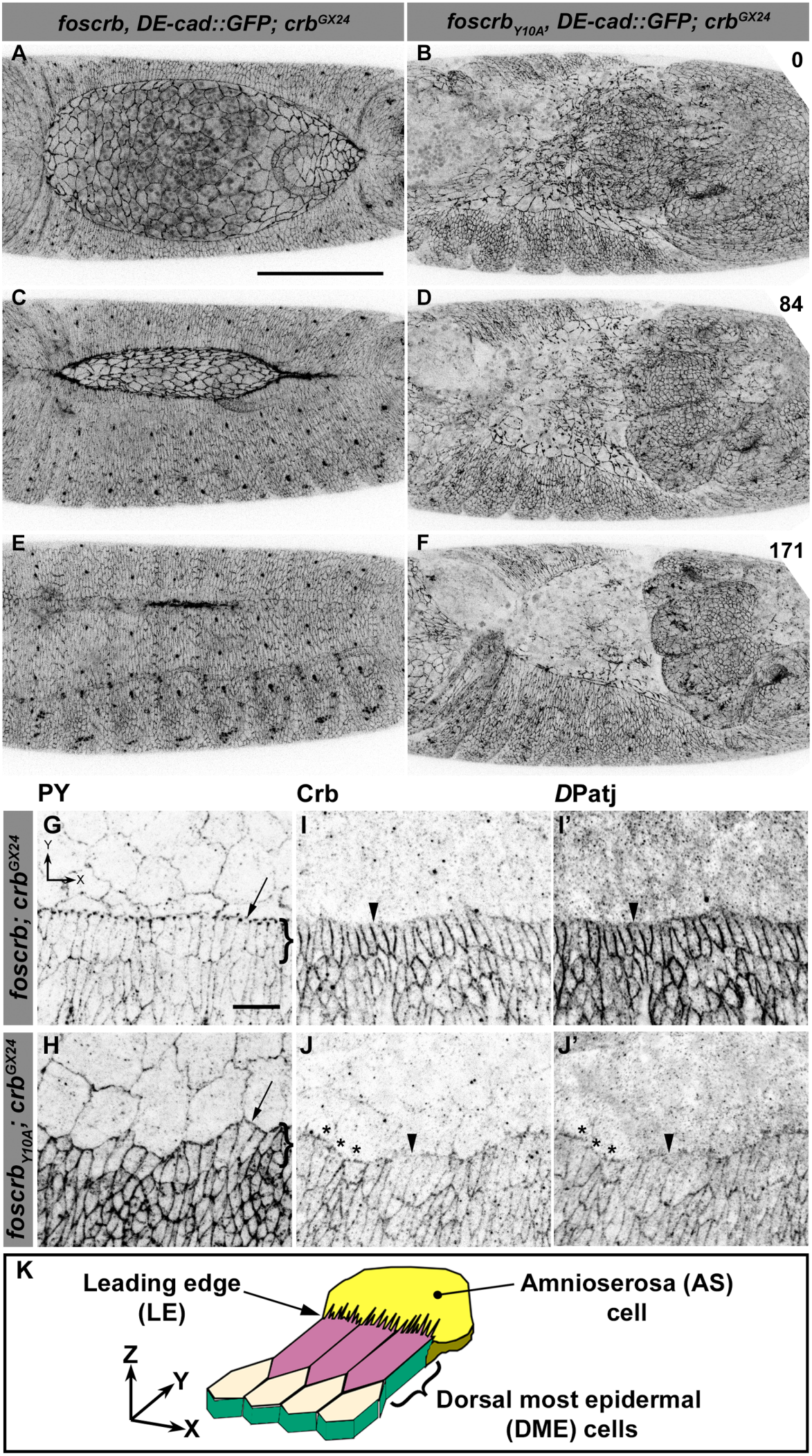
foscrb, DE-cad::GFP; crbGX24
foscrbY10A, DE-cad::GFP; crbGX24
A
B
0
C
D
84
E
F
171
PY
Crb
DPatj
foscrb; crbGX24
foscrbY10A; crbGX24
G
Y
X
I
I'
H
J
J'
K
Leading edge (LE)
Amnioserosa (AS) cell
Z
Y
X
Dorsal most epidermal (DME) cells

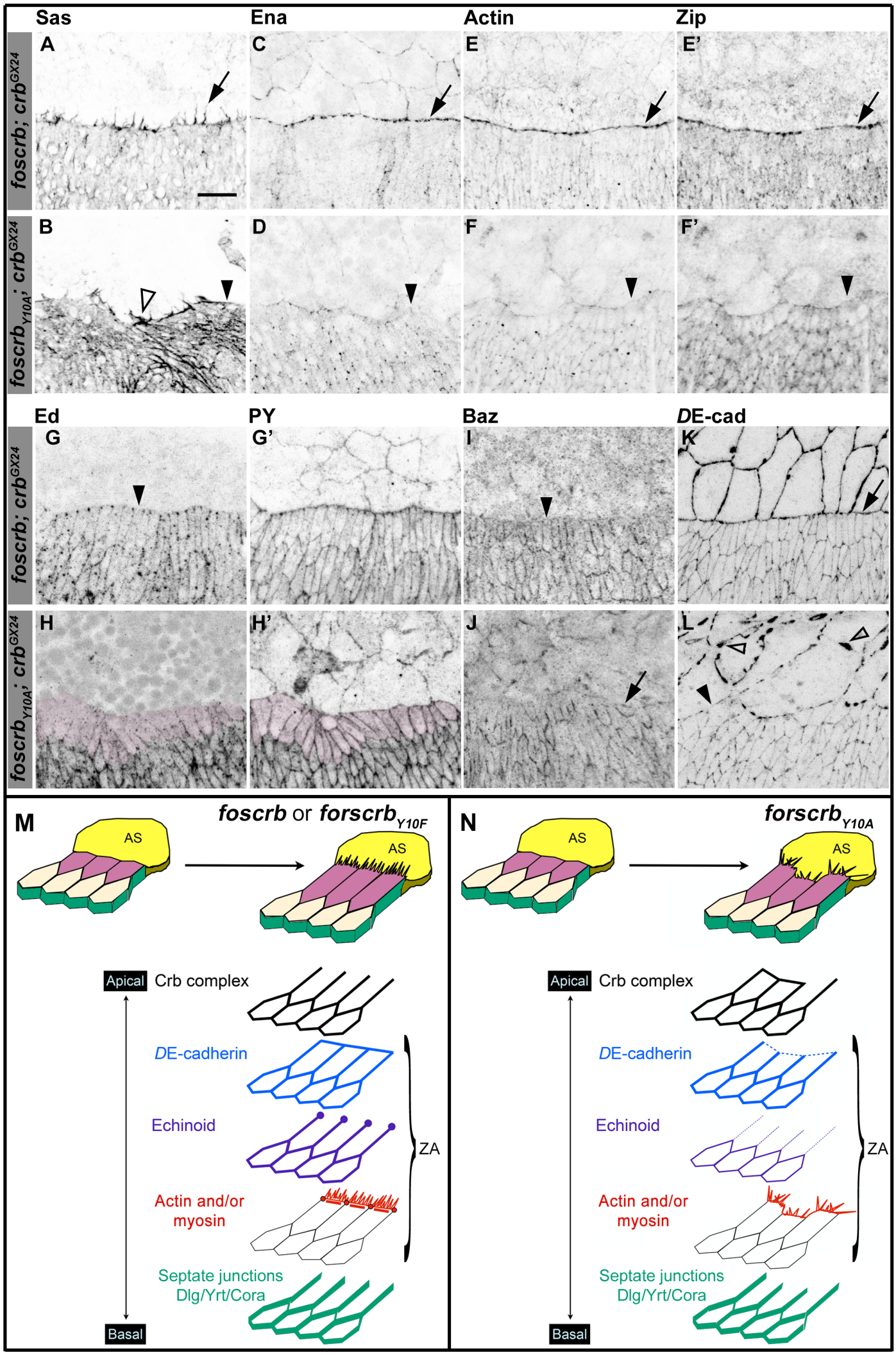
Sas
Ena
Actin
Zip
foscrb; crbGX24
foscrbY10A; crbGX24
A
B
C
D
E
E'
F
F'
Ed
PY
Baz
DE-cad
G
G'
H
H'
I
J
K
L
M
foscrb or forscrbY10F
AS
N
forscrbY10A
Apical
Crb complex
DE-cadherin
Echinoid
Actin and/or myosin
Septate junctions Dlg/Yrt/Cora
ZA
Basal

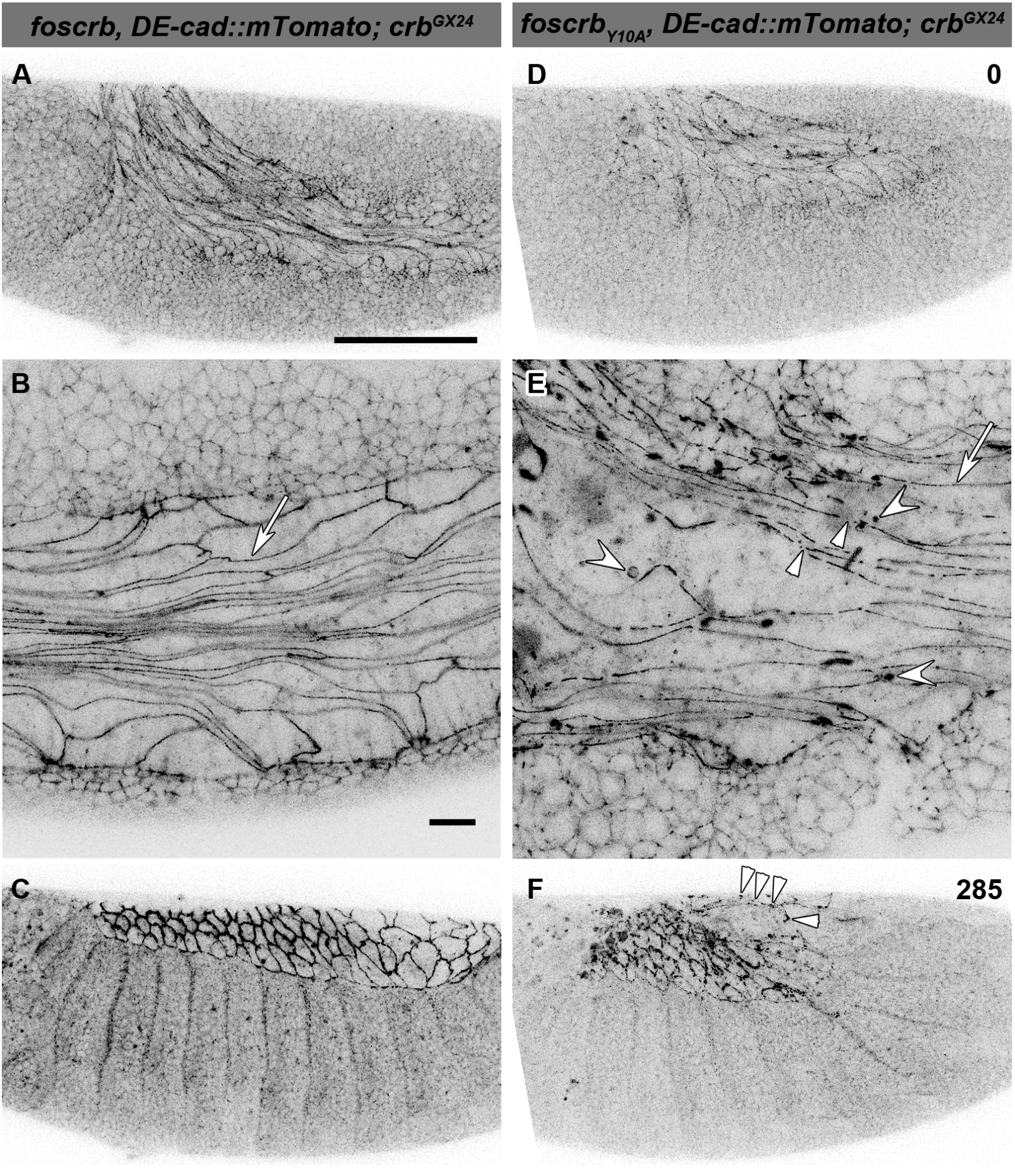
foscrb, DE-cad::mTomato; crb^GX24
foscrb_Y10A, DE-cad::mTomato; crb^GX24
A
B
C
D
0
E
F
285

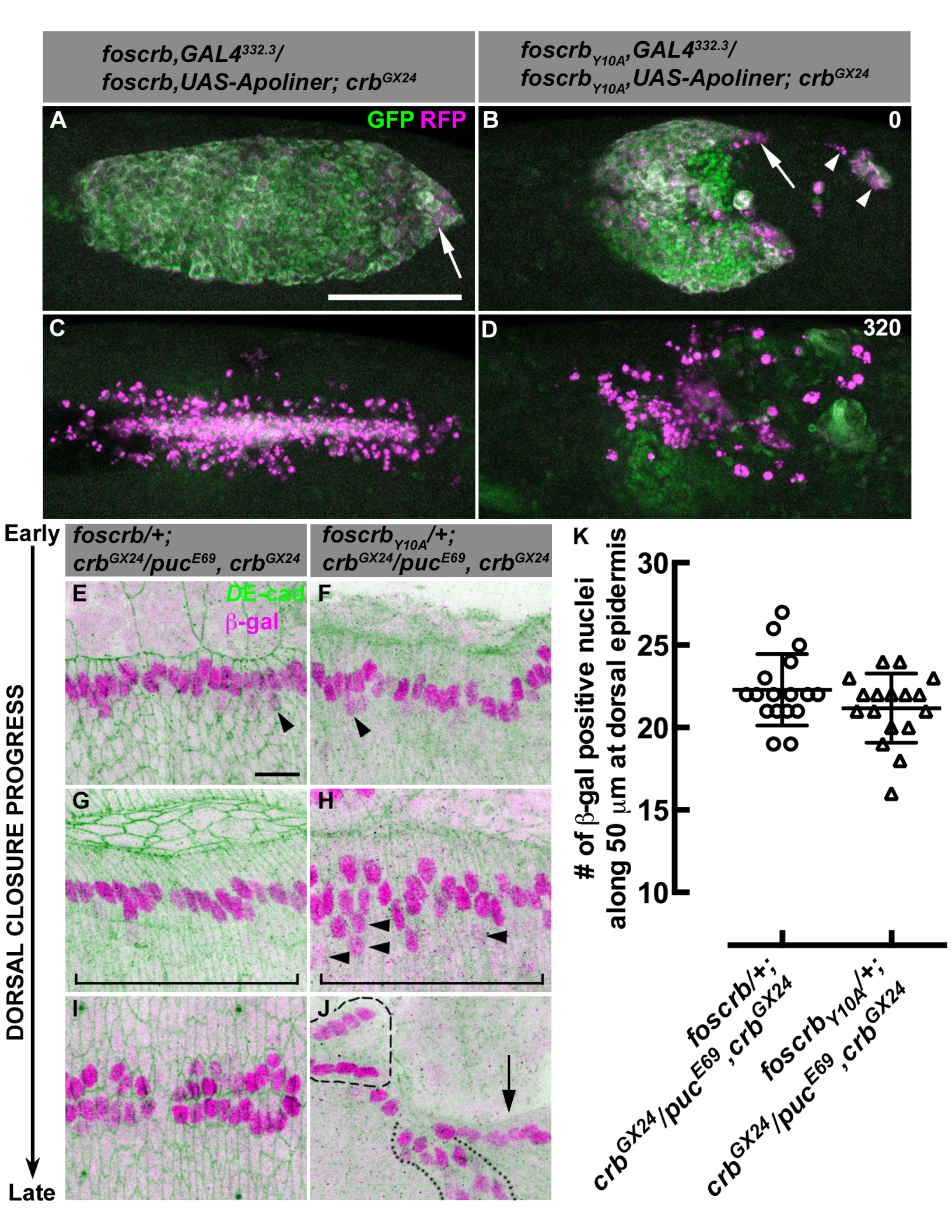
foscrb,GAL4332.3/
foscrb,UAS-Apoliner; crbGX24
foscrbY10A,GAL4332.3/
foscrbY10A,UAS-Apoliner; crbGX24
A
GFP RFP
B
0
C
D
320
Early
DORSAL CLOSURE PROGRESS
Late
foscrb/+;
crbGX24/pucE69, crbGX24
foscrbY10A/+;
crbGX24/pucE69, crbGX24
E
DE-cad
β-gal
F
G
H
I
J
K
# of β-gal positive nuclei
along 50 μm at dorsal epidermis
30
25
20
15
10
foscrb/+;
crbGX24/pucE69,crbGX24
foscrbY10A/+;
crbGX24/pucE69,crbGX24

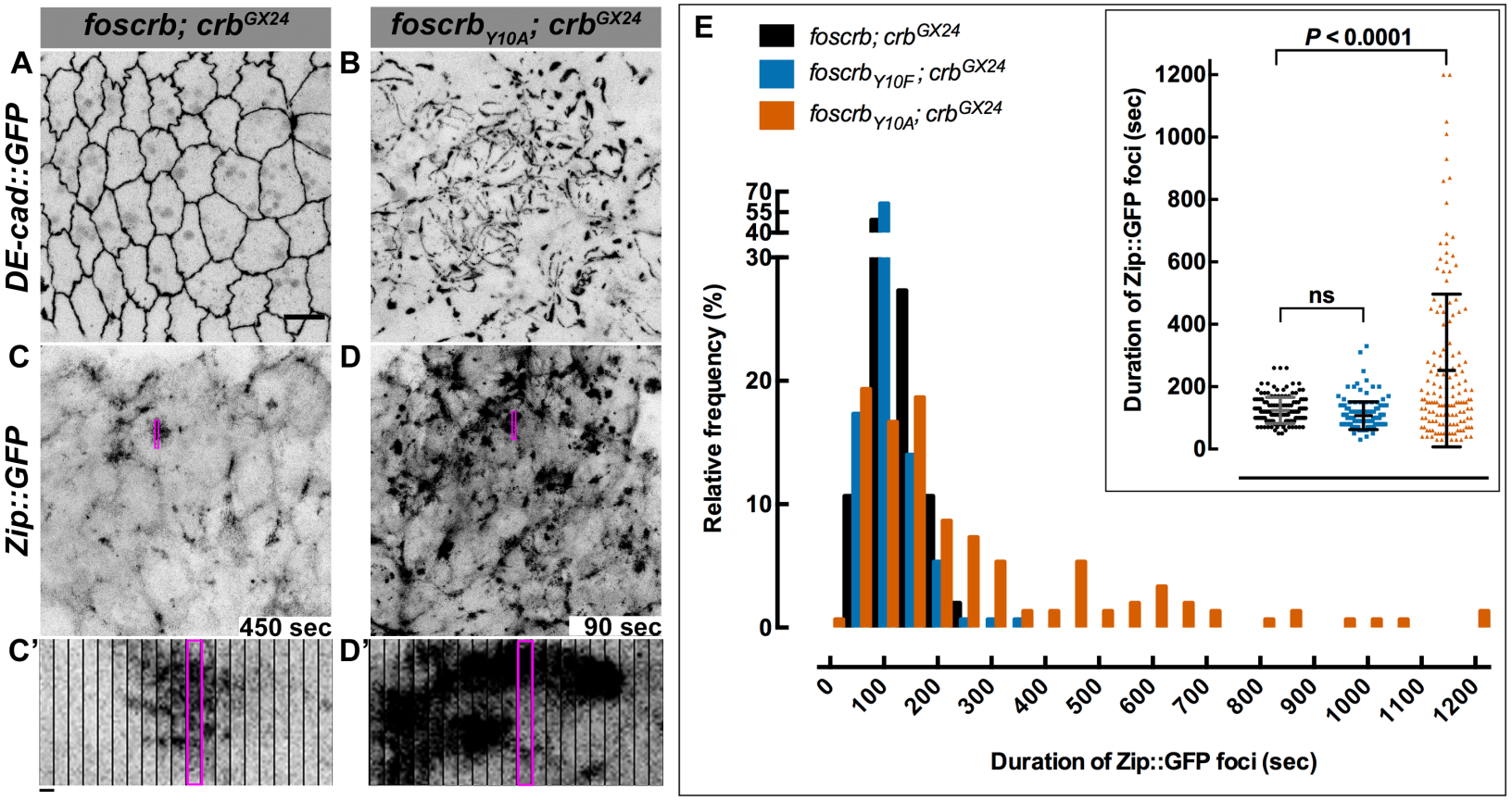
foscrb; crbGX24
foscrbY10A; crbGX24
A
B
DE-cad::GFP
C
D
Zip::GFP
450 sec
90 sec
C'
D'
E
foscrb; crbGX24
foscrbY10F; crbGX24
foscrbY10A; crbGX24
Relative frequency (%)
70
55
40
30
20
10
0
0
100
200
300
400
500
600
700
800
900
1000
1100
1200
Duration of Zip::GFP foci (sec)
P < 0.0001
ns
Duration of Zip::GFP foci (sec)
1200
1000
800
600
400
200
0

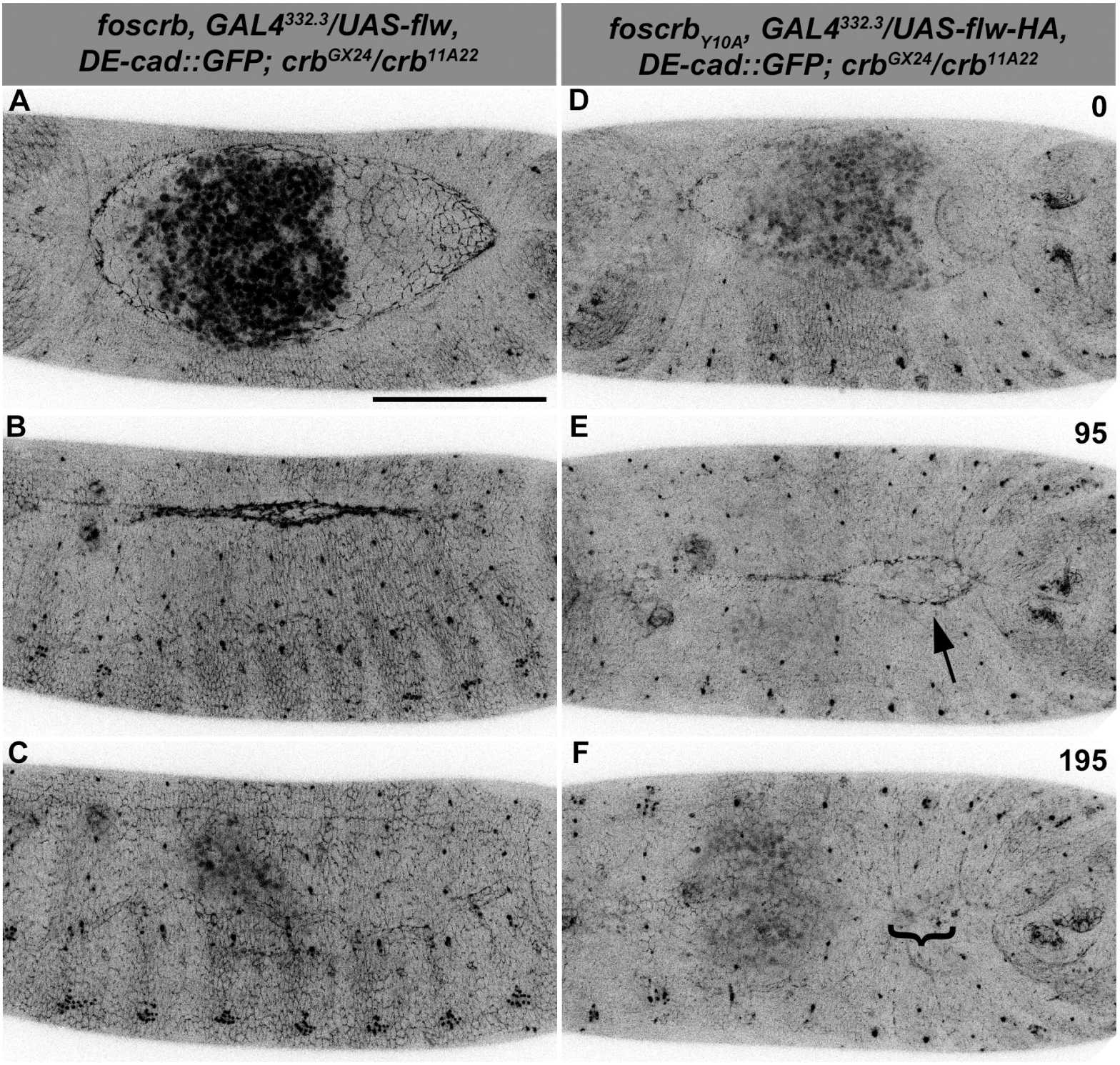
foscrb, GAL4332.3/UAS-flw,
DE-cad::GFP; crbGX24/crb11A22
foscrbY10A, GAL4332.3/UAS-flw-HA,
DE-cad::GFP; crbGX24/crb11A22
A
B
C
D
E
F
0
95
195

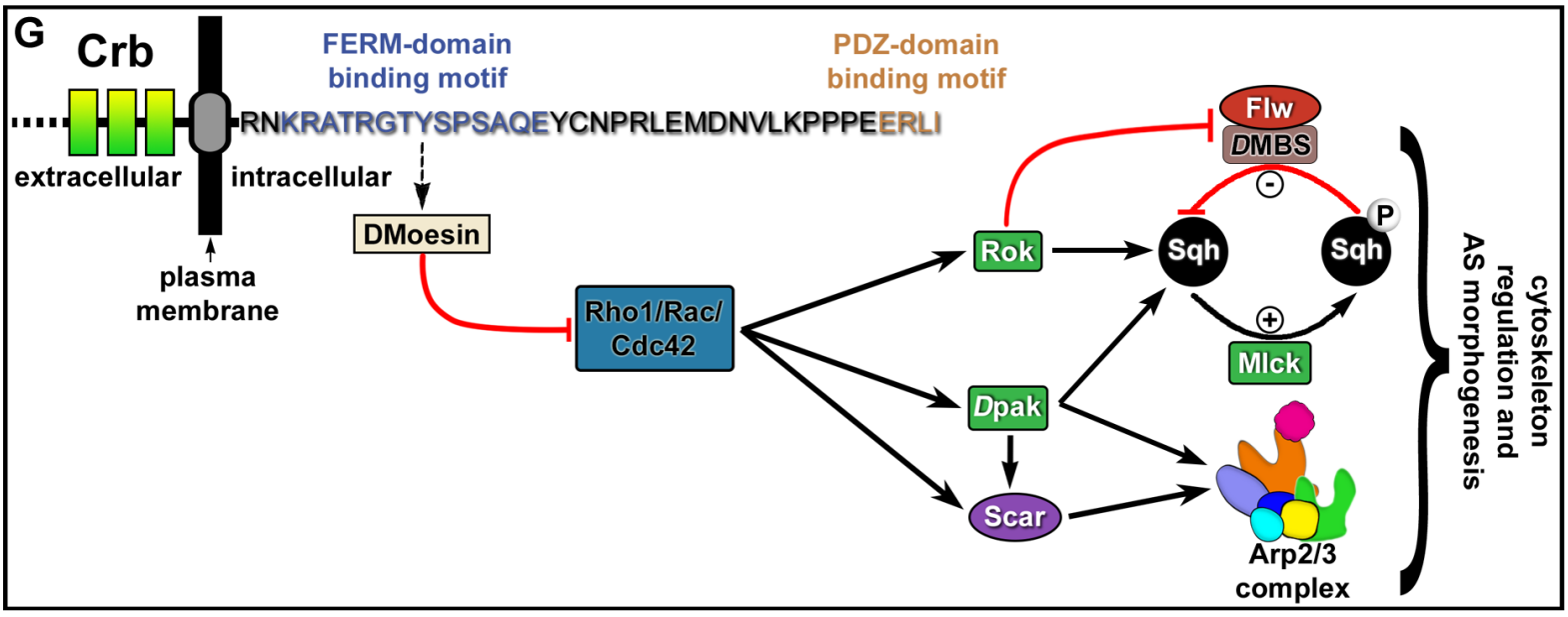
G
Crb
FERM-domain
binding motif
PDZ-domain
binding motif
RNKRATRGTYSPSAQEYCNPRLEMDNVLKPPPEERLI
extracellular
intracellular
plasma
membrane
DMoesin
Rho1/Rac/
Cdc42
Rok
Flw
DMBS
Sqh
Sqh
P
Mlck
Dpak
Scar
Arp2/3
complex
cytoskeleton
regulation and
AS morphogenesis

A

	crb allele	DE-cad::GFP	AS driver ($GAL4^{332.3}$)	UAS-Act::RFP	UAS-	others
1	GX24	-	-	-		
2	GX24	+	-	-		
3	GX24/11A22	+	-	-		
4	GX24	+	+	-		
5	GX24/11A22	+	+	-		
6	GX24/11A22	+	+	+		
7	GX24/11A22	-	+	-	UAS-Crb 29ºC	
8	GX24/11A22	-	+	-	UAS-Crb 25ºC	
9	GX24/11A22	-	+	-	UAS-Crb 18ºC	
10	GX24/11A22	+	+	+	UAS-flw-HA	
11	GX24/11A22	+	-	-		*flw*^{6}
12	GX24/11A22	+	+	-	UAS-Rho^{N19}	
13	GX24/11A22	+	+	-	UAS-rok-CAT-KG	
14	GX24	-	-	-		*Rho1*^{1B}
15	GX24/11A22	+	-	-		*rok*^{2}
16	GX24/11A22	+	+	-	UAS-Rac^{N17}	
17	GX24/11A22	+	+	+	UAS-*D*Pak-AID	
18	GX24/11A22	+	+	+	UAS-*D*Pak-myr	
19	GX24/11A22	+	+	+		
20	GX24/11A22	+	+	+	UAS-*D*moe^{T559D}	
21	GX24/11A22	+	+	-	UAS-*D*moe-myc	
22	GX24/11A22	+	+	+	UAS-*D*E-cad	
23	GX24	+	-	-		*SCAR*$^{\Delta 37}$/+
24	GX24/11A22	+	-	-		*Arp3*^{EP3640}/+
25	GX24/11A22	+	-	-		*Arp1*^{Q25st}/+

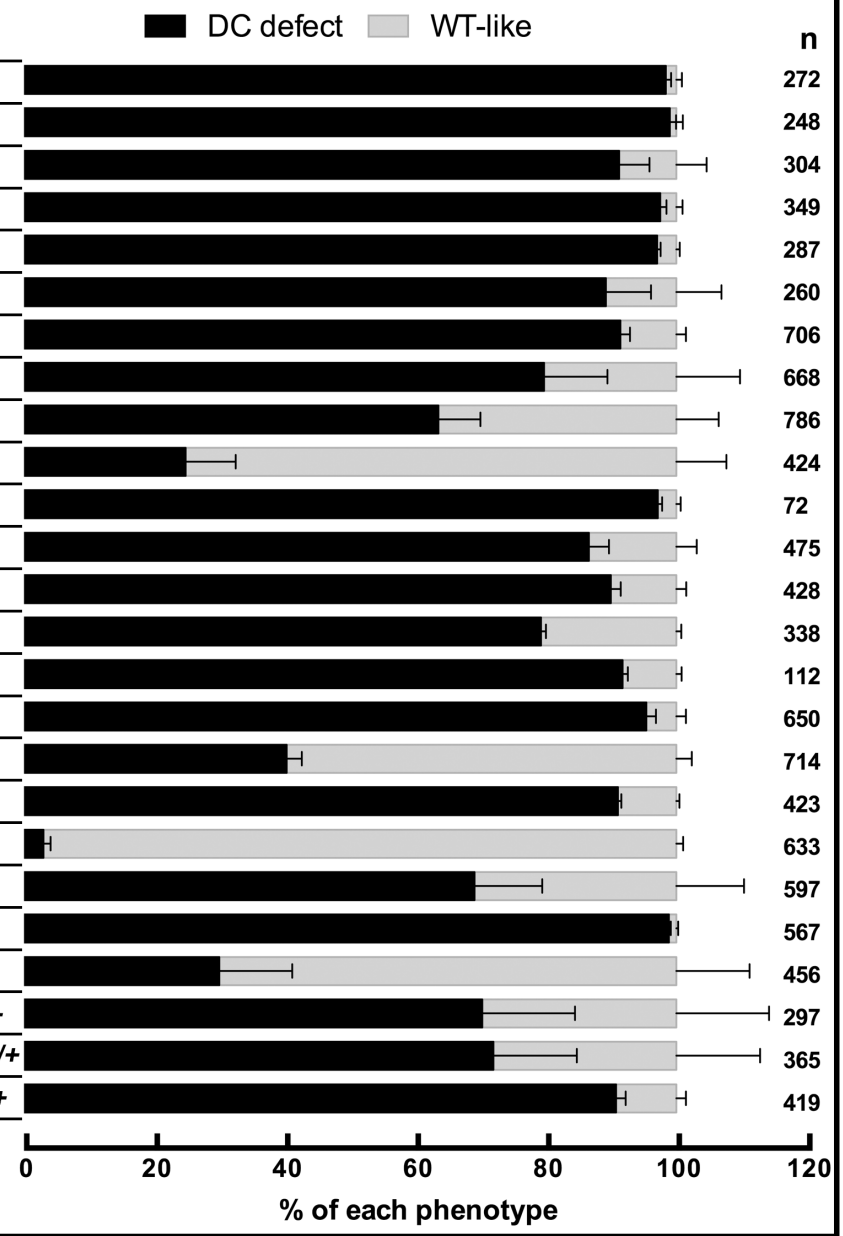

B

foscrb; crb^{GX24}

C

foscrb$_{Y10A}$*,GAL4*$^{332.2}$*/ UAS-flw-HA,DE-cad::GFP; crb*^{GX24}*/crb*^{11A22}*,UAS-Act::RFP*

D

foscrb$_{Y10A}$*,GAL4*$^{332.2}$*/ UAS-DPak-AID,DE-cad::GFP; crb*^{GX24}*/crb*^{11A22}*,UAS-Act::RFP*

E

foscrb$_{Y10A}$*,GAL4*$^{332.2}$*/ UAS-DE-cad,DE-cad::GFP; crb*^{GX24}*/crb*^{11A22}*,UAS-Act::RFP*

F

foscrb$_{Y10A}$*, DE-cad::GFP/ SCAR*$^{\Delta 37}$*,DE-cad::GFP; crb*^{GX24}

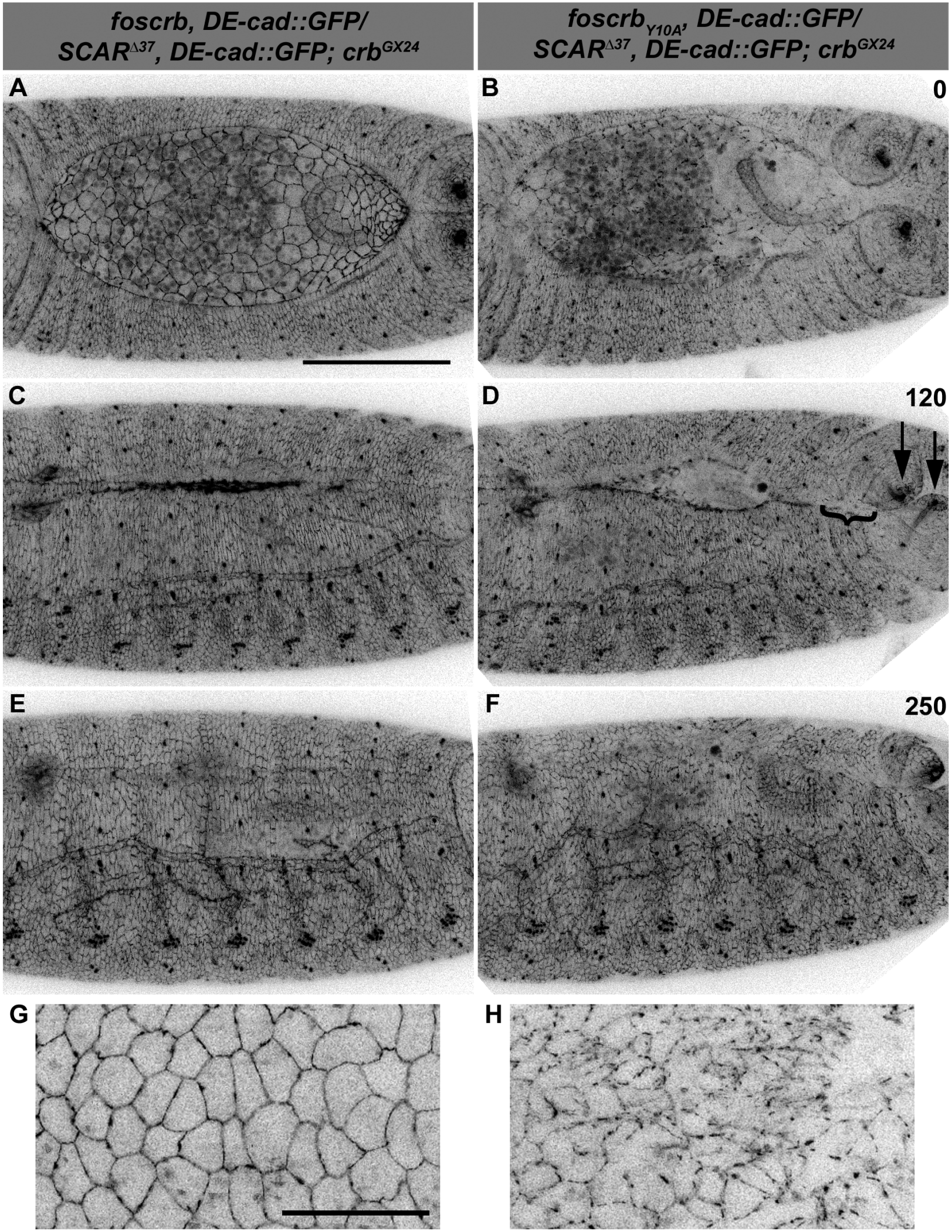
foscrb, DE-cad::GFP/
SCAR^Δ37, DE-cad::GFP; crb^GX24
foscrb_Y10A, DE-cad::GFP/
SCAR^Δ37, DE-cad::GFP; crb^GX24
A
B
0
C
D
120
E
F
250
G
H